Size effects in the crystal field of small dielectric particles of $SrCl_2$:Gd^{3+}

M. Rappaz,* C. Solliard, and A. Châtelain
Laboratoire de Physique Expérimentale, Ecole Polytechnique Fédérale de Lausanne, CH-1007 Lausanne, Switzerland

L. A. Boatner
Ecole Polytechnique Fédérale de Lausanne, CH-1007 Lausanne, Switzerland
and Solid State Division, Oak Ridge National Laboratory, Oak Ridge, Tennessee 37830
(Received 30 July 1979)

A technique based on evaporation in a viscous inert gas flow has been used to produce Gd^{3+}-doped $SrCl_2$ small particles whose average size varied from 100 to 500 Å. Electron paramagnetic resonance (EPR) investigations of these samples have shown that: (i) No observable phase separation occurred during the evaporation of Gd-doped crystals. (ii) The Gd^{3+} impurity ions occupied predominantly cubic-symmetry sites in the $SrCl_2$ small particles. (iii) The "small-particle" EPR spectrum of Gd^{3+} is characterized by significant differences relative to the spectrum observed in either a single crystal or a "large-grain" powder specimen. Such differences take the form of changes in the relative positions and widths of the EPR transitions. For the small-particle samples, the shifts and linewidths of the ⟨100⟩ shoulders in the EPR powder pattern were measured as a function of the average particle size. The observed shifts in the EPR lines are interpreted as arising from a contraction in the crystal lattice whose magnitude decreases with increasing particle size. This interpretation was confirmed by high-resolution electron-diffraction measurements. The heterogeneous broadening of the EPR lines was attributed to the effect of the particle size distribution as well as to internal strains and surface-related defects. By comparing the EPR and electron-diffraction results and using a simple "drop" model, it was possible to deduce a value of 0.435 N/m for the surface tension of $SrCl_2$ in the solid state. Similarly a power law for the b_4 spin-Hamiltonian parameter given by $b_4 \propto a^{-n}$ with $n = 18.7$ was determined. This exponent is about three times larger than the expected value. This work represents the first observation by EPR of crystallographic size effects in small dielectric particles.

I. INTRODUCTION

In the form of very small particles (10 to ~500 Å), solids exhibit physical, chemical, and electronic properties which differ significantly from the corresponding properties characteristic of the "bulk" material. Most of the previous theoretical and experimental work dealing with the physics of small particles has concentrated on the properties of metallic systems; and, as a result of these efforts, it is possible to distinguish two types of "size effects." These effects are: First the so-called "quantum size effect,"[1] where the normal "bulk" band structure of the metal is replaced by a series of discrete electronic levels which arise from a quantization due to the finite size of the metallic particle. Second, the "thermodynamic size effect," which arises from the emergence of surface effects due to the increased surface-to-volume ratio characteristic of finely divided solids. Experimental evidence for the "quantum" size effect has been provided by EPR,[2] NMR,[3] and optical investigations,[4] while the "thermodynamic size effect" has been detected in measurements of the vapor pressure,[5] specific heat,[6] thermal conductivity,[7] and melting point[8] of metallic small particles.

Electron-[9–12] and x-ray-[13–16] diffraction measurements have shown that surface effects can also produce changes in the lattice parameter of very small crystals. Although this "crystallographic" size effect was initially interpreted in terms of a simple average contraction of the lattice parameter, later results indicated that the actual effect was much more complicated. In fact, observations using high-resolution electron microscopy[17] have shown that small metallic particles (30 to 150 Å in diameter) are not single crystals but are characterized by what has been termed a "multitwinned" structure.[18] Such twinning can significantly affect the local strains in a crystal. Furthermore, the tensorial character of the surface stress has frequently not been included in "drop-model" interpretations of the diffraction patterns.

Although the technique of electron paramagnetic resonance has been employed in a number of investigations of size effects in small metallic particles, as noted above, the present work represents the first EPR observation of size effects in small dielectric par-

 ©1980 The American Physical Society

ticles.[19] Electron resonance is, of course, a well-known technique for investigations of the effects of crystalline electric fields on the energy levels of paramagnetic ions diluted in host crystals. The crystal-field parameters resulting from a "spin-Hamiltonian" analysis of the observed EPR spectra can frequently provide information concerning the local crystal-field strength and symmetry. These parameters are related to the distances between the paramagnetic ion and its neighbors. Power laws correlating the nearest-neighbor separation and the crystal-field parameters have been deduced from experiments involving the application of hydrostatic pressure,[20–22] uniaxial stress,[23,24] and temperature variations.[25,26] Even though the crystal-field parameters also reflect contributions due to such effects as overlap and covalency, the empirically determined variations as a function of nearest-neighbor distance show that paramagnetic impurities whose EPR spectrum is characterized by a significant crystal-field splitting can be employed as very sensitive probes for determining changes in the crystal field of the host material. Accordingly, the basic concept of the present work is to employ EPR measurements of small dielectric particles doped with paramagnetic impurities as a means of investigating crystallographic size effects. Information concerning defect concentrations and random strains in small dielectric particles can also be obtained from changes in the EPR linewidth. Additionally, by correlating the EPR results with electron-diffraction measurements and electron microscopy, it is possible to determine the coefficient in the power law relating the crystal-field parameters and the nearest-neighbor distance in small particles.

The fluorite-structure material $SrCl_2$ doped with the $^8S_{7/2}$ ground-state ion Gd^{3+} was chosen for the present studies for a variety of reasons, which are detailed in Sec. III. This section, which also presents the experimental techniques used to produce and measure the small Gd^{3+}-doped $SrCl_2$ particles, is preceded by a treatment of the formalism involved in calculations of the theoretical EPR powder spectrum for an $^8S_{7/2}$ system. In Sec. IV, the EPR and electron-diffraction results are presented; and a correlation of these measurements with the resulting conclusions is given in Sec. V.

II. THEORY

A. General

Trivalent gadolinium is characterized by a $(Xe)4f^7$ electronic configuration and accordingly has a ground state that is predominantly $^8S_{7/2}$. When this ion occupies a cubic substitutional site in a host such as $SrCl_2$, the EPR spectrum can be described by means of the following spin Hamiltonian:

$$\mathcal{H} = g\mu_B \vec{H}\cdot\vec{S} + \frac{b_4}{60}(O_4^0 + 5O_4^4) + \frac{b_6}{1260}(O_6^0 - 21O_6^4), \tag{1}$$

where μ_B is the Bohr magneton, b_4 and b_6 are the cubic crystal-field parameters, and the O_n^m are the Stevens operator equivalents. Lacroix[27] has calculated the exact eigenstates of this Hamiltonian when the magnetic field is applied along a $\langle 100\rangle$ crystallographic direction and has derived approximate expressions for a general orientation of the applied magnetic field. If the three direction cosines of the magnetic field relative to the $\langle 100\rangle$ crystallographic axes are denoted by l,m,n, then the magnetic field positions of the seven allowed transitions ($\Delta M_S = \pm 1$) are given by the following first-order expressions:

Transition	Notation	Position	Intensity
$\pm\frac{7}{2} \leftrightarrow \pm\frac{5}{2}$	$M = \pm\frac{7}{2}$	$H_M = \frac{1}{g\mu_B}(h\nu \mp 20pb_4 \mp 6qb_6)$	$I_M = 7$
$\pm\frac{5}{2} \leftrightarrow \pm\frac{3}{2}$	$M = \pm\frac{5}{2}$	$H_M = \frac{1}{g\mu_B}(h\nu \pm 10pb_4 \pm 14qb_6)$	$I_M = 12$
$\pm\frac{3}{2} \leftrightarrow \pm\frac{1}{2}$	$M = \pm\frac{3}{2}$	$H_M = \frac{1}{g\mu_B}(h\nu \pm 12pb_4 \mp 14qb_6)$	$I_M = 15$
$+\frac{1}{2} \leftrightarrow -\frac{1}{2}$		$H_0 = \frac{h\nu}{g\mu_B}$	$I_0 = 16$

(2)

where

$$p = 1 - 5(l^2m^2 + m^2n^2 + n^2l^2) ,$$

$$q = \tfrac{21}{2}[11l^2m^2n^2 - (l^2m^2 + m^2n^2 + n^2l^2) + \tfrac{2}{21}] .$$

B. Powder spectrum

In the present work, measurements of the crystal-field parameters b_4 and b_6 which appear in the spin Hamiltonian [Eq. (1)] will be made as a function of the $SrCl_2$:Gd^{3+} crystallite size. Accordingly, the Gd^{3+} ions will not be dispersed in one single macroscopic crystal, but will occupy sites in numerous small randomly oriented particles. Therefore, the EPR spectrum does not consist of seven lines corresponding to the seven allowed transitions $\Delta M_S = \pm 1$ appropriate to a single orientation of the applied magnetic field, but represents an average over all possible magnetic field orientation in accordance with the angular relations given in Eqs. (2). The resulting EPR "powder" spectrum can be calculated by a technique developed in this section. A simple interpretation of EPR powder spectra can be obtained by using the method of Lagrangian multipliers.[28] This method, which is outlined in Appendix A, does not provide intensity information but does predict the positions of the singularities which correspond to the "peaks" (i.e., the shoulders and divergences) in the powder spectrum.

A general expression for a single-crystal spectrum (including, of course, the spectrum of Gd^{3+}) can be written as follows:

$$I^S(H) = \sum_M I_M^S(H) = \sum_M I_M \cdot \mathcal{F}_M[H - H_M(l,m,n)] \ , \tag{3}$$

where I_M and $H_M(l,m,n)$ are, respectively, the intensity and the position of the EPR line (M) which is given to first order by the expressions (2), and $\mathcal{F}_M(H)$ is a normalized line shape [i.e., $\int_{-\infty}^{+\infty} \mathcal{F}_M(H) \times dH = 1$]. Using the Dirac δ function, we can rewrite $I_M^S(H)$ as:

$$I_M^S(H) = I_M \int_{-\infty}^{+\infty} \delta[H' - H_M(l,m,n)] \cdot \mathcal{F}_M(H - H')\, dH' \ . \tag{4}$$

If the spectrum of the paramagnetic ion (or center) in the powder sample is "isotropic", then the corresponding intensity $I_M^P(H)$ of the line (M) in the powder spectrum can be expressed as the following average:

$$I_M^P(H) = \frac{1}{4\pi} \int_\Omega I_M^S(H)\, d\Omega \ , \tag{5}$$

where Ω is a sphere of unit radius and $d\Omega$ the element of solid angle. Assuming that the intensity I_M and the line shape $\mathcal{F}_M(H)$ are independent of the orientation (l,m,n) of the magnetic field, then the expression (5) will be transformed into

$$I_M^P(H) \sim \int_{-\infty}^{+\infty} I_M^{P\delta}(H')\mathcal{F}_M(H - H')\, dH' = [I_M^{P\delta}(H) * \mathcal{F}_M(H)] \ , \tag{6}$$

where

$$I_M^{P\delta}(H') = I_M \int_\Omega \delta[H' - H_M(l,m,n)]\, d\Omega \ . \tag{7}$$

The function $I_M^{P\delta}(H)$ simply represents the powder-spectrum intensity of a very sharp line (M). Using the properties of the Dirac δ function, it can be shown that Eq. (7) is equivalent to

$$I_M^{P\delta}(H) = I_M \frac{1}{dH} \int_\Omega d\Omega \ , \tag{8}$$

with the condition $H \leq H_M(l,m,n) \leq H + dH$ and with

$$d\Omega = \sin\theta\, d\theta\, d\phi = -d(\cos\theta)\, d\phi = -dn\, d\phi \ .$$

By making the change of variables given by

$$n \rightarrow n \ ,$$

$$\phi \rightarrow H = H_M(l,m,n) = H_M[\phi = \arctan(m/l), n] \ ,$$

we obtain the following result:

$$I_M^{P\delta}(H) = -I_M \int \frac{dn}{(\partial H/\partial\phi)_n} \ , \tag{9}$$

with $H = H_M(\phi,n)$. This expression may now be rewritten into the following final form:

$$I_M^{P\delta}(H) = I_M \int \frac{dn}{m(\partial H/\partial l) - l(\partial H/\partial m)} \ , \tag{10}$$

with the conditions

$$l^2 + m^2 + n^2 = 1 \ , \quad H = H_M(l,m,n) \ .$$

This result is quite general and applies to any powder-spectrum calculation. Although the function to be integrated over the parameter n in Eq. (10) is not complicated in general, the limits of the integration are not well known, since they are implicitly given by the two conditions under which the integration must be performed. In an actual computer simulation of a powder spectrum, considerable computation time can be saved by using the two conditions given in Eq. (10) to express l and m as functions of H and n. Using the first-order expressions (2) which are appropriate to an $^8S_{7/2}$ ion in a cubic site, it is possible to fix the position of each line (M) relative to the $(-\frac{1}{2} \rightarrow +\frac{1}{2})$ central line and to express the relative magnetic field position H in the following form:

$$H = H_M(l,m,n) = \alpha_M p + \beta_M q \ , \tag{11}$$

where p and q are defined in Eqs. (2) and α_M, β_M are coefficients proportional to $b_4/g\mu_B$ and $b_6/g\mu_B$, respectively. In Appendix B a derivation is given which shows that, in this case, the powder spectrum intensity is given by the following expression:

$$I_M^{P\delta}(h_M) \sim \frac{I_M}{(\frac{5}{2}\alpha_M + \frac{21}{4}\beta_M)} \int \frac{dn}{f_M(n,h_M)} \ , \tag{12}$$

with

$$f_M(n,h_M) = (2n^4-2n^2+1-h_M)^{1/2} \times [2h_M-(3n^4-2n^2+1) - \epsilon_M n^2(n^4-2n^2+1)]^{1/2} ,$$

$$\epsilon_M = \frac{231\beta_M}{10\alpha_M+21\beta_M} ,$$

$$h_M = \frac{H+(\frac{3}{2})\alpha_M+(\frac{17}{4})\beta_M}{(\frac{5}{2})\alpha_M+(\frac{21}{4})\beta_M} ,$$

where h_M equals the "reduced field." In this form, the limits of the above integration are explicitly given by the domain of definition of the function $f_M(n,h_M)$. For $\epsilon_M=0$ (i.e., $b_6=0$), this domain is simply defined by the zeros of the two biquadratic expressions which appear in the function f_M. The domain of definition is shown in Fig. 1 together with the contour lines of the function $f_M^{-1}(n,h_M)$. Regarding this figure, it should be noted that the reduced field h_M can only vary from $\frac{1}{3}$ to 1. The value $h_M=1$ (or $H=\alpha_M$) is only satisfied for $n=0, \pm 1$, and by using the two conditions which apply to Eq. (10), it can be shown that this extremum corresponds only to the ⟨100⟩ directions. Similarly, the extremum $h_M=\frac{1}{3}$ (or $H=-\frac{2}{3}\alpha_M$) is obtained only for the applied magnetic field parallel to the ⟨111⟩ directions. These extrema, which are in agreement with those found by using the method of Lagrangian multipliers (cf. Appendix A), give rise to "shoulders" in the powder-spectrum intensity, since, for these points, the integral in Eq. (12) has a finite value. The value $h_M=\frac{1}{2}$ (or $H=-\frac{1}{4}\alpha_M$) for which the integral diverges near $n=0$ and $n=\pm 1/\sqrt{2}$, corresponds to a "divergence" of $I_M^{P\delta}(H)$. This divergence, which does not arise uniquely from the ⟨110⟩ directions [n varies continuously from $-(2/3)^{1/2}$ to $+(2/3)^{1/2}$], will be denoted by a ⟨110⟩ symbol.

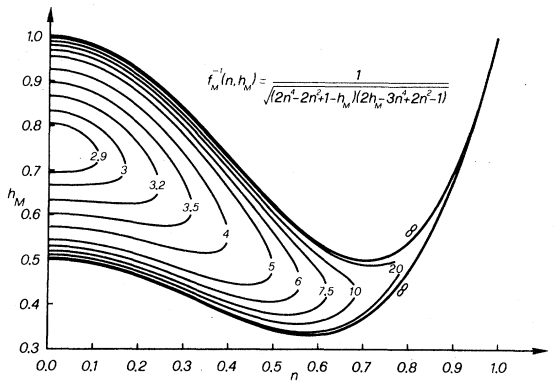

FIG. 1. Domain of definition and contour lines for the function $f_M^{-1}(n,h_M)$ which must be integrated over the parameter n at constant h in order to obtain the intensity $I_M^{P\delta}(H)$. Although this function diverges at the limits of the domain, the integration in Eq. (12) only gives rise to a divergence in the powder spectrum for $h_M=\frac{1}{2}$, $(n=0, \pm 1/\sqrt{2})$. (It should be noted that, since the function $f_M(n,h_M)$ is symmetric in n, only half of the complete domain is shown.)

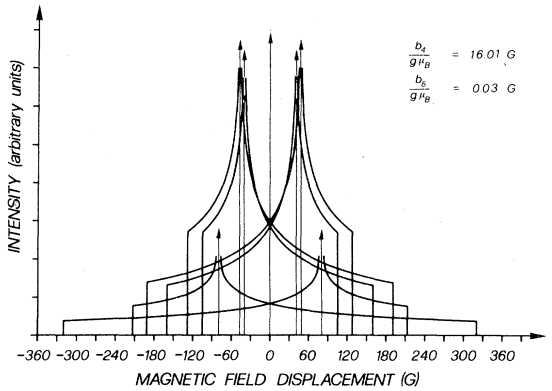

FIG. 2. Calculated EPR powder spectrum of $SrCl_2$:Gd^{3+}. The intensity $I_M^{P\delta}(H)$ of the line M has been calculated by integrating the function $f_M^{-1}(n,h_M)$ in accordance with Eq. (12). For each line (except the $-\frac{1}{2} \rightarrow +\frac{1}{2}$ transition), the two shoulders ⟨100⟩ and ⟨111⟩ and the divergence ⟨110⟩ are shown. The values of g, b_4, and b_6 are those determined by Abraham *et al.* Ref. (29).

When $\epsilon_M \neq 0$, as shown in Appendix C, the two shoulders and the divergence always occur for the same crystallographic directions and only the extremum $h_M=\frac{1}{3}$ above is transformed into $h_M=(9+2\epsilon_M)/27$. The result of the numerical integration of Eq. (12) is shown in Fig. 2 for the seven individual lines corresponding to the $\Delta M_S=\pm 1$ transitions in an $^8S_{7/2}$ state. The values of b_4 and b_6 used in this calculation were obtained by Abraham *et al.*[29] for the $SrCl_2$:Gd^{3+} system. By performing the convo-

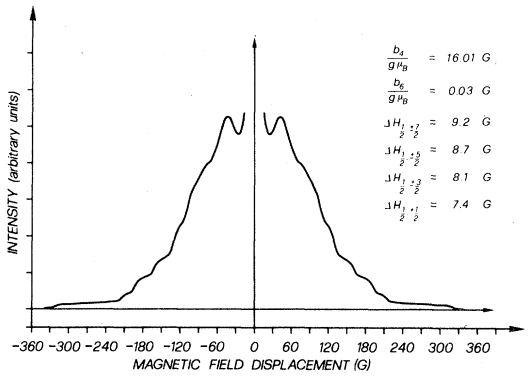

FIG. 3. Calculated convoluted EPR absorption powder spectrum for $SrCl_2$:Gd^{3+}. The convolution of Eq. (6) has been performed by using the results illustrated in Fig. 2 and Lorentzian line shapes whose full width at half maximum $\Delta H_{1/2,M}$ was measured from the single-crystal EPR spectrum.

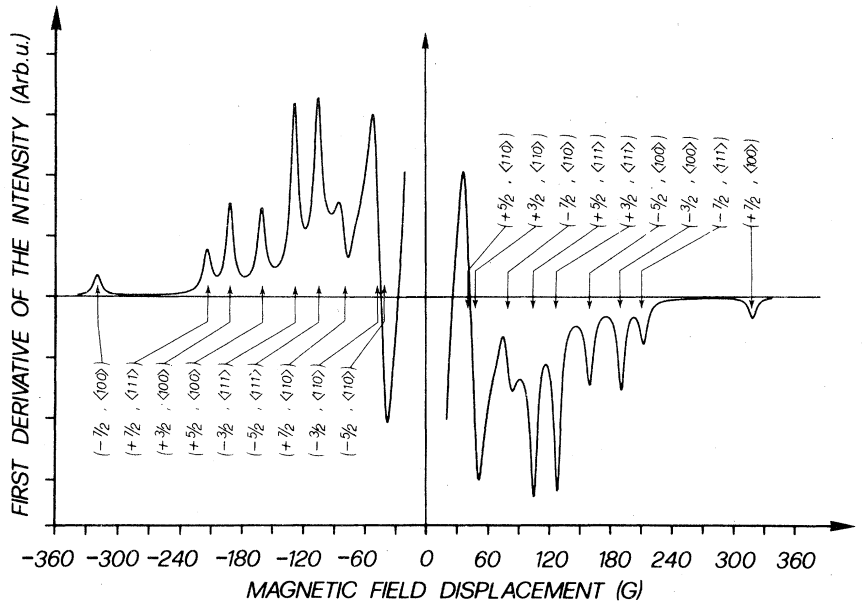

FIG. 4. First derivative of the calculated convoluted $SrCl_2:Gd^{3+}$ EPR powder spectrum. The positions of shoulders and divergences are indicated on the figure. This theoretical spectrum can be compared with the experimental spectrum shown in Fig. 8.

lution of Eq. (6) with Lorentzian line shapes, the absorption powder spectrum $I^P(H) = \sum_M I^P_M(H)$ and its corresponding first derivative can be computed, and the results of such calculations are shown in Figs. 3 and 4, respectively. The "theoretical" first derivative EPR powder spectrum shown in Fig. 4 is to be compared with the experimental spectrum presented in Sec. IV A (i.e., Fig. 8).

A calculation of the parameters g, b_4, and b_6 is usually carried out using data obtained from a single-crystal EPR spectrum with the magnetic field positions measured at the zero crossing of the first derivative of the EPR lines. For a powder spectrum, however, an identical determination is not trivial, and the following considerations are very useful: (i) If the intensity $I^{P\delta}_M(H)$ has the very simple form of a Heaviside function $I^{P\delta}_M(H) = Au(H - H_u)$, then the convolution (6) is such that

$$\frac{dI^P_M(H)}{dH} = A\mathfrak{F}_M(H - H_u) \quad . \tag{13}$$

(ii) In Fig. 2 it is apparent that near a $\langle 100 \rangle$ shoulder the slope of $I^{P\delta}_M(H)$ is very small. If the line shape is much narrower than the total spread of the line in the powder spectrum, Eq. (13) is to be used. Consequently, the $\langle 100 \rangle$ shoulders in the first derivative of the EPR powder spectrum are equivalent to the lines observed for $\vec{H} \| \langle 100 \rangle$ in the single-crystal absorption spectrum. (iii) The expressions for the energy levels given by Lacroix[27] when $\vec{H}$ is applied along a $\langle 100 \rangle$

TABLE I. Magnetic field separation $\Delta H^{(2)}_{M,\langle 100 \rangle}$ between the two symmetric shoulders-$(+M \leftrightarrow +M-1, \langle 100 \rangle)$ and $(-M \leftrightarrow -M+1, \langle 100 \rangle)$ as directly deduced from Eqs. (2) and (14), and $\Delta H^{\text{meas}}_{M,\langle 100 \rangle}$ as "measured" on the convoluted theoretical spectrum of Fig. 4. The values of g, b_4 and b_6 are those determined by Abraham *et al.* (Ref. 29).

M	$\Delta H^{(2)}_{M,\langle 100 \rangle}$	$\Delta H^{(2)}_{M,\langle 100 \rangle}$ (G)	$\Delta H^{\text{meas}}_{M,\langle 100 \rangle}$ (G)	Relative error
$\frac{7}{2}$	$\frac{1}{g\mu_B}\lvert 40b_4 + 12b_6 \rvert$	640.80	640.99	0.03%
$\frac{5}{2}$	$\frac{1}{g\mu_B}\lvert 20b_4 + 28b_6 \rvert$	321.12	320.92	−0.06%
$\frac{3}{2}$	$\frac{1}{g\mu_B}\lvert 24b_4 - 28b_6 \rvert$	383.32	382.99	−0.09%

direction can be used in second order. If the field H_M is replaced in the second-order terms by the central field H_0, then: (a) the g value is given, to second order, by the expression

$$g = \frac{h\nu}{\mu_B}\left(\frac{H_{5/2}+H_{-5/2}}{2}\right)^{-1}, \tag{14a}$$

since there are no second-order terms for the $\pm\frac{5}{2} \leftrightarrow \pm\frac{3}{2}$ transitions; and (b) the splitting between the lines $H_{+M,\langle 100\rangle}$ and $H_{-M,\langle 100\rangle}$ is the same in first and second order

$$\Delta H^{(2)}_{M,\langle 100\rangle} = |H^{(2)}_{+M,\langle 100\rangle} - H^{(2)}_{-M,\langle 100\rangle}| = \Delta H^{(1)}_{M,\langle 100\rangle}, \tag{14b}$$

since the second-order terms are the same for $(+M)$ or $(-M)$.

The relationship shown in Eq. (13) is well satisfied for the powder spectrum of $SrCl_2$:Gd^{3+}. This is evident from an examination of the data shown in Table I, where the second-order theoretical splitting $\Delta H^{(2)}_{M,\langle 100\rangle}$ and the splitting "measured" from the convoluted spectrum of Fig. 4 are shown. Finally, it should be noted that the equivalence between the powder-spectrum shoulders and the single-crystal lines is still valid in the case of inhomogeneous line broadening.

III. EXPERIMENTAL

A. System selection

An EPR investigation of crystallographic size effects in insulating solids involves studies of "powder" samples consisting of an ensemble of small dielectric particles containing paramagnetic impurities or centers. The production of such small-particle samples by means of an evaporation technique and interpretation of the associated results can be facilitated significantly by choosing a system which meets certain criteria. Some of the more pertinent of these criteria are as follows:

(i) *The dielectric host material must be relatively easy to evaporate and must not dissociate during the evaporation process.* The vapor pressure of $SrCl_2$ is listed as $P = 4\times10^{-3}$ torr at 1245 K,[30] and $P = 760$ torr at 2273 K.[31] Values of the $SrCl_2$ vapor pressure obtained by extrapolation between these two points appear to be consistent with our observations and permit evaporations of $SrCl_2$ to be made at realistic temperatures. (It should be noted that the value for the boiling point of $SrCl_2$ listed as 1523 K in Ref. 32 does not appear to be reasonable in view of the evaporation rates observed in the present work.) Dissociation of $SrCl_2$ can occur via the reaction $SrCl_2 + H_2O \rightarrow SrO + 2HCl$, but this reaction only takes place in the presence of water and at temperatures of 873 K or greater.[33,34] In the evaporation system used in the present work, the partial pressure of H_2O vapor was less than 10^{-6} torr.

(ii) *Significant phase separation between the host dielectric and the paramagnetic "probe" impurities must not occur during the evaporation process.* The rare-earth halides are known to be highly soluble in the alkaline-earth halides[35] [e.g., for the system $(SrCl_2)_{1-x}(EuCl_3)_x$, x can vary from 0 to 0.23].[36] This high solubility is undoubtedly a significant factor in the absence of any observed phase separation in the $SrCl_2$:Gd evaporations carried out in the course of the present investigation.

(iii) *The host dielectric should have a crystallographic structure that is both simple and unique.* Strontium chloride only crystallizes with the cubic fluorite structure ($a_0 = 6.9767$ Å).[37] [It should be noted that a diffuse transition has been observed at 973 K.[38] Between this temperature and the melting point of $SrCl_2$ (1146 K), the Cl^- ions are characterized by a high mobility in a rigid lattice of Sr^{2+}.]

(iv) *The paramagnetic "probe" ion should occupy only one site in the host material.* In the absence of the deliberate addition of other impurities, only the cubic site EPR spectrum of Gd^{3+} is observed in $SrCl_2$.[29] The Gd^{3+} ions occupy substitutional Sr^{2+} sites, and the observation of a cubic spectrum indicates that the necessary charge compensation does not occur close to the paramagnetic impurity. This situation is in marked contrast to that found for the other alkaline-earth halides, where trigonal, tetragonal, and orthorhombic symmetry spectra are frequently in evidence.[39,40]

(v) *The characteristic spectrum of the paramagnetic impurity ion should not exhibit significant hyperfine (or superhyperfine) structure.* Hurren[21] has shown that in the case of Eu^{2+} in the alkaline-earth fluorides, the hyperfine structure is not sensitive to changes in the lattice parameter, and accordingly such structure simply results in a needless complication of the EPR spectrum. Only two of the Gd isotopes have a nuclear spin and the measured hyperfine interactions for these isotopes are small, i.e., $\sim 5\times10^{-4}$ cm^{-1}.[41,42] (The isotopes are ^{155}Gd with $I=\frac{3}{2}$ and a natural abundance of 14.73% and ^{157}Gd with $I=\frac{3}{2}$ and a natural abundance of 15.68%.[43])

(vi) *The crystal-field splitting of the ground-state energy levels should not be too large.* In an EPR powder spectrum, the intensities represent an effective average over all possible orientations of the applied magnetic field relative to the randomly oriented crystallites which form the powder. Accordingly, large magnetic field separations result in reduced powder-spectrum intensities. For Gd^{3+} in $SrCl_2$ the maximum magnetic field spread occurs between the $\pm\frac{7}{2} \leftrightarrow \pm\frac{5}{2}$ transitions when $\vec{H}$ is applied along a $\langle 100\rangle$ crystallographic direction, and this spread is only about 640 G.[29]

A consideration of the above factors resulted in the selection of $SrCl_2$ as the small-particle host system and of Gd^{3+} as the paramagnetic impurity ion. It is clear that the criteria listed above represent a fairly restrictive set of conditions and, therefore, that it is unlikely that a large number of systems amenable to studies of this type will be found. Finally, it should be noted that $SrCl_2$ has the highly undesirable characteristic of being very hygroscopic. Accordingly, in the form of a small-particle sample or powder any contact with moist air must be avoided.

B. Sample preparation

Gadolinium-doped $SrCl_2$ single crystals were grown for the specific purpose of providing dry, high-purity, homogeneously doped starting material for the production of small-particle samples by means of an evaporation process. These single crystals were grown by a standard Bridgman technique from carefully mixed $SrCl_2$ and $GdCl_3$ powders which had been dehydrated by slowly heating the mixture under vacuum to a temperature of 673 K. This dehydrated mixture was transferred under vacuum to the quartz growth ampoule which had been degassed previously by heating under vacuum for 48 hours at 1173 K. The resulting $SrCl_2:Gd^{3+}$ single crystals not only provided feed material for the small-particle evaporations but were also used to produce "bulk" (i.e., large-grain) reference powder samples by means of simple mechanical grinding.

The gas-evaporation technique originally developed by Kimoto *et al.*[44,45] produces small particles by thermalizing the vapor phase in a low pressure of a cooler inert gas, and the size of the resulting particles depends on the evaporation rate, the pressure and nature of the gas, and the geometry of the evaporation chamber. This technique was chosen because fast thermalization of the vapor atoms, which experience an average of 3 to 4 impacts with the inert-gas atoms,[46] serves to prevent phase separation between the dielectric host material and the paramagnetic impurities. This characteristic alone is not a sufficient criterion, however, since the concentrations of the two vapor phases still must be equivalent to those in the starting material. Due to the high solubility of the rare earths in the alkaline-earth halides, this latter condition seems to be satisfied automatically for $SrCl_2:Gd^{3+}$. For other systems (e.g., $CaF_2:Mn^{2+}$ which was investigated initially) a standard evaporation process distills the Mn^{2+} ions, and flash-evaporation techniques are required.[46]

In contrast to the technique of evaporation on a substrate,[8] the gas-evaporation technique also has the advantage of producing small particles which are directly formed in a crystalline state. In fact, as shown by Solliard *et al.*[17] for small gold particles, a subsequent anneal is not required in order to bring the small particles to thermodynamic equilibrium. Due to natural convection phenomena, however, the gas-evaporation technique does give rise to large particle-size distributions. This size distribution can be reduced by employing a cylindrical furnace through which the gas is pumped.[47,48] This pro-

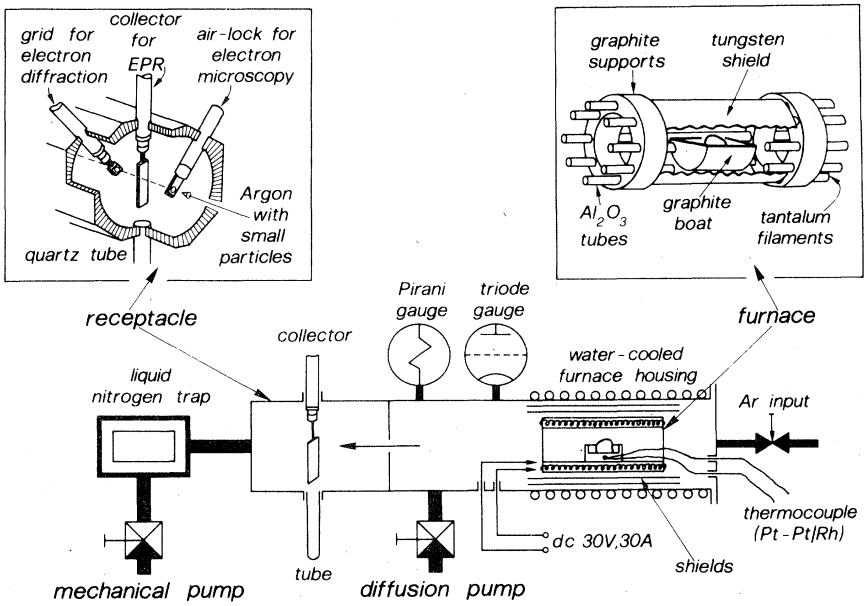

FIG. 5. Schematic diagram of the apparatus used to produce small $SrCl_2:Gd^{3+}$ particles. A single crystal of $SrCl_2:Gd^{3+}$ (0.5%) was placed in the graphite boat inside the furnace and evaporated in a viscous flow of pure argon (5*N*7). The small particles, which were formed by condensation, were transported by the gas flow through diaphragms to the collection chamber.

cedure also continuously renews the gas and eliminates degassed impurities. Additionally, the small particles which are transported by the viscous gas flow can be collected easily.

The apparatus used to produce the small $SrCl_2$:Gd^{3+} particles investigated in this work is shown schematically in Fig. 5. A horizontal configuration was chosen for the cylindrical furnace shown in Fig. 5, since the free surface of the $SrCl_2$ crystal does not radiate toward a cool region in this case and, accordingly, a more uniform evaporation temperature is obtained.

Prior to each evaporation, the apparatus was degassed at 343 K for 48 hours under a vacuum of 3×10^{-6} torr. Simultaneously, the furnace temperature was slowly increased in order to eliminate traces of H_2O absorbed on the surface of the $SrCl_2$:Gd^{3+} single crystal, which was contained in a graphite boat. Beginning at a temperature of about 773 K the walls of the chamber were water cooled. The temperature of the furnace was then increased to 1373 K. When the chamber pressure was below 10^{-5} torr, the diffusion pump was isolated and the argon circuit opened. At this point the argon (*5N7* purity) was pumped through a liquid-nitrogen trap using an ordinary mechanical pump. In the present case the argon flow was maintained in the viscous regime, in contrast to the technique described previously in Refs. 46 and 49. Since aerodynamic problems can arise when collecting small particles, the argon-flow conditions were fixed at an argon pressure of 10 torr and an argon flow rate of 5.62 torr l/sec. When the evaporation temperature was reached, the small particles formed by condensation of the vapor were transported by the argon flow and deposited on the various collectors illustrated in Fig. 5. Once the samples were collected, the chamber was repumped to 3×10^{-6} torr and the samples were sealed.

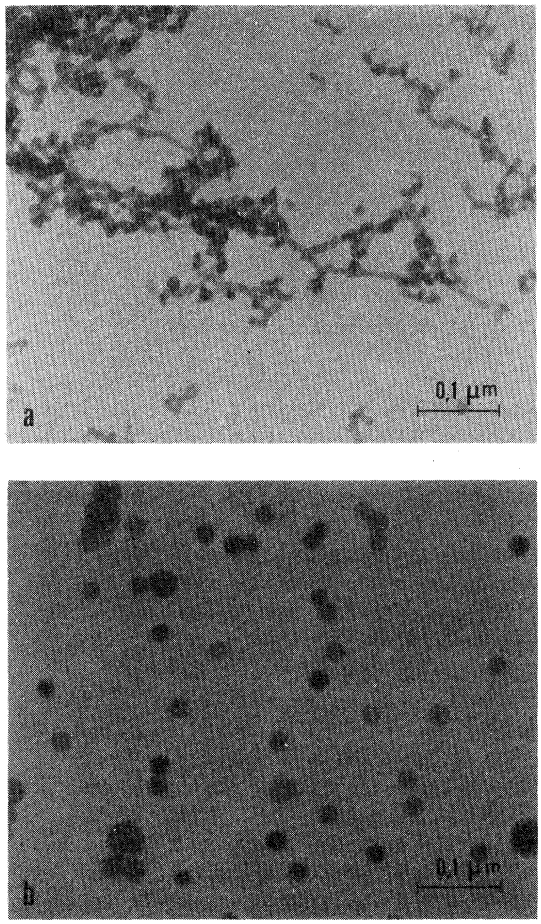

FIG. 6. Electron micrographs of the small $SrCl_2$:Gd^{3+} particles produced with the apparatus illustrated in Fig. 5. The argon pressure (10 torr) and flow rate (5.62 torr l/sec) are the same for the two samples. In this way, the average size ϕ_v of the particles can be controlled by the evaporation temperature alone. (a) $T_e = 1373$ K and $\phi_v = 100$ Å; (b) $T_e = 1658$ K and $\phi_v = 250$ Å. It should be noted that the smallest particles, as shown in *a*, are arranged in chainlike structures, while the larger particles illustrated in *b* are well isolated.

Electron micrographs of small $SrCl_2$:Gd^{3+} particles produced by the technique described above are shown in Fig. 6 for two evaporation temperatures. The smallest particles (mean diameter $\phi_v = 100$ Å) are apparently aggregated in "chainlike" strands. This structure is not specific to strontium chloride and has also been observed for CaF_2,[46] PbI_2,[48] some oxides, and other small dielectric particles.[50] The preference for forming these "chainlike" aggregates is not completely understood at the present time, but it is presumably related to surface dipolar effects. Using electron micrographs such as those shown in Fig. 6, it is difficult to obtain size histograms and, consequently, the samples are best characterized by the mean individual particle diameter ϕ_v.

C. Measurement techniques

In order to eliminate any contact with moist air, the small $SrCl_2$ particles were collected directly on a quartz plate for the EPR measurements. The details are illustrated in Fig. 5. This plate was attached to a feed-through which had a double *O*-ring seal and could be introduced under vacuum into a quartz tube (diameter 11 mm) by using a sliding rod. The feed-through then ensured the integrity of the vacuum in the quartz tube. In this way it was possible to transfer the small particles under vacuum to the EPR spectrometer. Prior to every sample deposition, the quartz tube and plate were outgassed at 773 K for 48 hours.

The EPR measurements were performed with a standard *X*-band Varian *E*-line spectrometer. The microwave frequency and magnetic field were mea-

sured using an *EIP*-350*D* counter and an automatic proton gaussmeter (Bruker *BNM*-12). Each shoulder observed in the powder spectrum was "detailed" (i.e., spread in magnetic field) in order to precisely fix its position and linewidth. The recorded shoulder was digitized with a *HP*-9864*A* digitizer which was connected to a Hewlett-Packard 9830*A* calculator. This calculator then provided the input to a *CDC* 3600 computer. In this way, it was possible to send the digitized values to the computer automatically, fit them with a Lorentzian line shape superimposed on a linear base, return the adjusted parameters to the calculator, and finally transform them into the shoulder position and linewidth by using two proton references which were also digitized.

The sample-deposition technique used in the electron-diffraction measurements was identical to that described above for the EPR studies, except that the quartz plate was replaced by a standard electron-microscope grid which was coated with a thin carbon film. The vacuum seal was broken inside the diffractograph (after it was evacuated) by using a sliding rod. A moving furnace was used to anneal the sample *in situ* without moving the microscope grid.

Small dielectric particles produced by evaporation on a heated substrate do not form the chainlike structures shown in Fig. 6(a) and are well isolated. Therefore, in order to establish more accurately the relationship between the particle size and lattice parameter, measurements were also performed on samples prepared by *in situ* evaporation on a substrate.[8] In this case, the grid was attached to an air-lock system[51] so that it could be directly transferred under vacuum to the electron microscope. Contrary to the case of the formation of small metal particles, the substrate must be heated to about 773 K when evaporating $SrCl_2$ if well-isolated small particles and high-quality Debye-Scherrer diffraction patterns are desired. When the evaporation of the $SrCl_2$ was performed on a substrate at room temperature, an amorphous film was formed. Annealing this film at 773 K resulted in the appearance of spotted rings in the diffraction pattern, which indicated that a crystalline film had been produced. The electron-diffraction measurements were performed with a *KD*4-Balzers diffractograph (50 kV), and the analysis of the plates was identical to that described in Ref. 9. Thallium chloride was always used as a reference.

Electron micrographs of the small $SrCl_2$ particles were obtained with a high-resolution Philips *EM*-300*S* transmission microscope, and the air-lock system previously described in Ref. 51 was used to transfer the sample under vacuum.

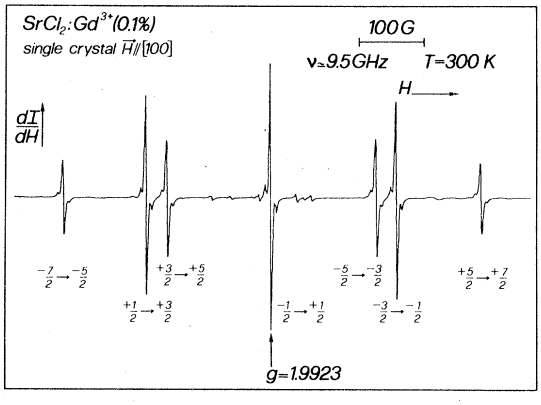

FIG. 7. First derivative EPR spectrum for a $SrCl_2$:Gd^{3+} (0.1%) single crystal as obtained at *X*-band and room temperature when $\vec{H}$ is applied along a [100] direction. The satellite lines on each side of the seven main lines are due to the hyperfine structure associated with $Gd^{155}(I=\frac{3}{2}$, natural abundance 14.73%) and $Gd^{157}(I=\frac{3}{2}$, natural abundance 15.68%). The observed line shapes for this spectrum were used to perform the theoretical convolution of Eq. (6).

IV. RESULTS

A. $SrCl_2$:Gd^{3+} single crystals and large-grain powders

The EPR spectrum of a Gd^{3+}-doped $SrCl_2$ crystal (grown as described in Sec. III B) is shown in Fig. 7 for $\vec{H}\|[100]$. The linewidths of the various electronic transitions were used to obtain the convoluted theoretical spectra shown in Figs. 3 and 4. Equations (2) and (14) were used to calculate the spin-Hamiltonian parameters from the measured line positions. The results are listed in Table II and are in good agreement with the previously reported results of Abraham *et al.*[29] For the $-\frac{1}{2} \rightarrow +\frac{1}{2}$ "central" transition, as shown in Fig. 7, it was possible to resolve partially the hyperfine structure of the ^{155}Gd and ^{157}Gd isotopes. The measured hyperfine constants for these two isotopes are listed in Table II.

Figure 8 shows the experimentally determined EPR powder spectrum of $SrCl_2$:Gd^{3+} (0.5%) which was obtained at room temperature ($\sim$297 K) and *X* band. The agreement with the computed "theoretical" spectrum shown in Fig. 4 is apparently quite good. It should be pointed out, however, that one must take into account the fact that the line shape $F_M(H)$, which enters into the convolution of Eq. (6), depends on the orientation of the applied magnetic field. As noted by Abraham *et al.*,[29] for a nonprincipal direction, the superhyperfine structure due to the Cl neighbors is partially resolved. This coupling together with second-order effects can introduce additional structure on the two superimposed divergences $(+\frac{1}{2} \rightarrow +\frac{3}{2}, \langle 110\rangle)$ and $(+\frac{3}{2} \rightarrow +\frac{5}{2}, \langle 110\rangle)$. Ef-

TABLE II. Spin-Hamiltonian parameters of $SrCl_2$:Gd^{3+} at X-band and room temperature.

Samples (figure No.)	g	$(-)b_4$ (10^{-4} cm^{-1})	$(-)b_6$ (10^{-4} cm^{-1})	$\frac{A_{155}}{A_{157}}$ (10^{-4} cm^{-1})
Single crystal (Ref. 29)	1.9925 ±0.0005	14.89 ±0.02	0.031 ±0.004	. . . . .
Single crystal (7)	1.9915 ±0.0005	14.99 ±0.02	0.019 ±0.01	3.81 ±0.1 5.05 ±0.1
Powder (8)	1.9918 ±0.0005	14.99 ±0.02	0.020 ±0.01	. . . . .
Sample with $\phi_v = 100$ Å annealed at 673 K (10)	1.9915 ±0.0005	14.99 ±0.02	0.030 ±0.01	. . . . .
Sample with $\phi_v = 250$ Å (13)	1.9913 ±0.0005	15.07 ±0.02	0.023 ±0.01	. . . . .

fects due to the partially resolved superhyperfine structure are more pronounced when the Gd^{3+} concentration is lowered to 0.1%. Second-order terms, which have not been taken into account in the present powder-spectrum calculations, can slightly modify the positions of shoulders and divergences. They will also significantly affect the $(-\frac{1}{2} \rightarrow +\frac{1}{2})$ transition. This transition, which is nonsymmetric at X-band, is perfectly symmetric at the higher Ka-band frequency. It is possible to distinguish weak structure on both sides of the $-\frac{1}{2} \rightarrow +\frac{1}{2}$ line even in the powder spectrum. This structure corresponds to the values $M_I = \pm\frac{3}{2}$ for the Gd^{155}- and Gd^{157}-hyperfine structure. The "powder-spectrum" spin-Hamiltonian parameters listed in Table II have been deduced by measuring the positions of the $\langle 100 \rangle$ shoulders. These values are in agreement with those measured for the single-crystal sample.

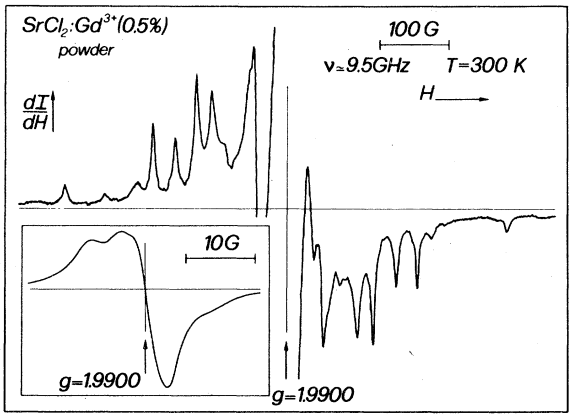

FIG. 8. First derivative of the $SrCl_2$:Gd^{3+} (0.5%) EPR powder spectrum obtained at X band and room temperature. The central line corresponding to the $-\frac{1}{2} \rightarrow +\frac{1}{2}$ transition is about 100 times more intense than the other fine structure lines and is shown at reduced gain in the corner of the figure. This line is nonsymmetric due to second-order effects. This experimental spectrum is to be compared with the "theoretical" spectrum shown in Fig. 4.

B. Small particle samples

The EPR spectrum shown in Fig. 9 was obtained for the small-particle sample whose electron micrograph is shown in Fig. 6(a) (mean diameter: $\phi_v = 100$ Å). The lines are obviously considerably broadened, and only the shoulders ($\pm\frac{3}{2} \leftrightarrow \pm\frac{1}{2}$, $\langle 100 \rangle$) are still well resolved. Consequently, it was not possible to deduce directly the spin-Hamiltonian parameters for this sample. If one considers the general form of the spectrum, however, and, in particu-

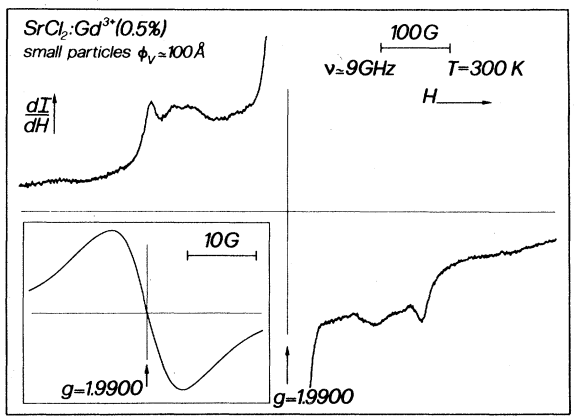

FIG. 9. EPR spectrum corresponding to the small-particle sample whose electron micrograph is shown in Fig. 6(a) (mean diameter $\phi_v = 100$ Å). The g value of the central line is the same as that of the ground, large-grain powder sample (see Fig. 8), but the fine-structure lines are considerably broadened and slightly shifted, as shown in detail in Fig. 11.

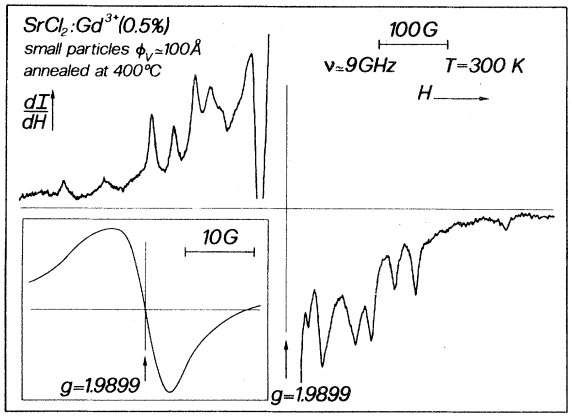

FIG. 10. EPR spectrum corresponding to the small-particle sample used for Fig. 9 after annealing at 400°C for 3–4 minutes. The lines are now well resolved, and the spin-Hamiltonian parameters obtained for this spectrum are identical within experimental error to those determined for large-grain samples (see Table II).

lar, makes comparisons of the positions of the shoulders $(\pm\frac{7}{2}\leftrightarrow\pm\frac{5}{2},\langle 100\rangle)$ and $(\pm\frac{5}{2}\leftrightarrow\pm\frac{3}{2},\langle 100\rangle)$, it can be seen that the Gd^{3+} ions are predominantly still in cubic symmetry sites in the small $SrCl_2$ particles. If the sample is annealed at 673 K for 2 to 4 minutes, the spectrum shown in Fig. 10 is obtained, and the lines are again well resolved. The spin-Hamiltonian parameters obtained for this sample are indicated in Table II, and they correspond exactly to those found for "bulk" samples (i.e., for either single crystal or ground, large-grain powders.)

Figure 11 shows the details of the shoulders

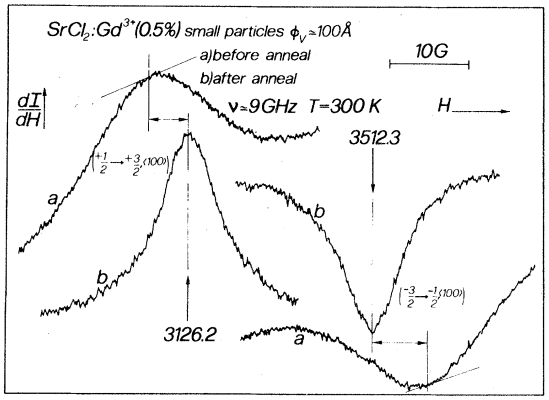

FIG. 11. Detail of the shoulders $(\pm\frac{3}{2}\leftrightarrow\pm\frac{1}{2},\langle 100\rangle)$ in the EPR spectra shown in Figs. 9 and 10 for $SrCl_2$:Gd^{3+}, $\phi_v = 100$ Å, before and after annealing. The positions of the lines as deduced by fitting with Lorentzian line shapes superimposed on a linear base are shown on the figure. The shift of the shoulders which occurs for the small-particle sample is clearly evident in this figure.

$(\pm\frac{3}{2}\leftrightarrow\pm\frac{1}{2},\langle 100\rangle)$ which correspond to the spectra shown in Figs. 9 and 10. By fitting these shoulders as described in Sec. III C, it is possible to calculate the magnetic field separation $(\Delta H_{3/2,\langle 100\rangle})$ between the $(-\frac{3}{2}\rightarrow-\frac{1}{2},\langle 100\rangle)$ and $(+\frac{1}{2}\rightarrow+\frac{3}{2},\langle 100\rangle)$ transitions. For the small-particle sample whose mean diameter ϕ_v was 100 Å, this separation was determined to be 11.5 G larger than that found for the large-grain powder specimens. This increased magnetic field separation corresponds to an increase of about 3% in the b_4 spin-Hamiltonian parameter for the small-particle sample relative to the "bulk" value.

In order to confirm that a size effect is actually being observed, it is obviously necessary to vary the particle size in a systematic way and to correlate the changes in b_4 with the particle size. EPR and electron-diffraction measurements which establish such a correlation will be presented in Secs. IV C and IV D. Prior to presenting these results, however, some additional experimental results and associated arguments will be given which clearly show that the increased b_4 parameter observed in the spectrum shown in Fig. 9 is due to a size effect:

(i) *The shift of the shoulders* $(\pm\frac{3}{2}\leftrightarrow\pm\frac{1}{2},\langle 100\rangle)$ *is not an artifact due to overlapping broadened lines.* This possibility is eliminated as discussed in Appendix D. The positions and linewidths of these shoulders have been measured as a function of Gd^{3+} concentration for "bulk" powder samples, and a subsequent analysis shows that the overlap of broadened lines does not shift their position.

(ii) *The increased* b_4 *parameter is correlated with a decrease in the lattice parameter a.* Figure 12 shows the electron-diffraction profiles corresponding to the small-particle sample whose EPR spectra are shown in Figs. 9 (before annealing) and 10 (after annealing). Prior to the anneal, the diffraction peaks exhi-

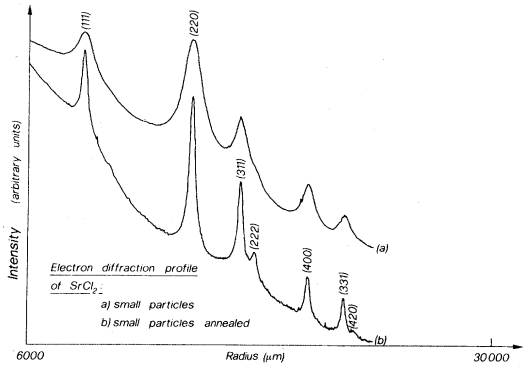

FIG. 12. Electron-diffraction profiles of small $SrCl_2$:Gd^{3+} particles corresponding to the electron micrograph shown in Fig. 6(a) (mean diameter $\phi_v = 100$ Å). Profile (a) corresponds to the EPR spectrum of Fig. 9 (before anneal) and profile (b) to the annealed sample whose EPR spectrum is shown in Fig. 10.

bit, in addition to a broadening, a small shift as compared with the diffraction peaks for the annealed sample. From measurements made using the (400) Debye-Scherrer ring, it was possible to determine that the observed shift corresponds to a contraction of the lattice parameter of $\Delta a/a = -0.2\%$ in the small-particle sample. This result yields a power law for b_4 given by $\Delta b_4/b_4 = -n(\Delta a/a)$ with $n \sim 15$.

(iii) *The anneal increases the size of the particle* [as indicated by the electron-diffraction profiles shown on Fig. 12 (Ref. 52)], and b_4 *resumes its bulk value following this anneal.* The objection could be made, however, that the anneal could also change the density and the repartition of defects inside the crystals (e.g., anionic Frenkel defects or chlorine vacancies filled with impurities, etc.)

(iv) *When the evaporation temperature is increased, the size of the* $SrCl_2$ *particles is increased and the corresponding EPR spectrum tends to the bulk powder spectrum shown in Fig. 8.* This is shown in detail in the next sections; as an example, the spectrum shown in Fig. 13 corresponds to the electron micrographs of Fig. 6(b) ($\phi_v = 250$ Å, $T_e = 1658$ K). The lines are well resolved and the spin-Hamiltonian parameters deduced for this sample and listed in Table II indicate that the relative change $\Delta b_4/b_4$ is only 0.5%. (It should be noted that it would be very improbable for a concentration of defects created during the evaporation process to decrease with increasing evaporation temperature.)

(v) *A simple collapse of the small particles eliminates the shift* Δb_4. If the sealed quartz tube containing the small-particle sample is opened for a short period of time, contact with the moist air not only results in some hydration, but the small particles collapse into large aggregates. (An example of this collapse for

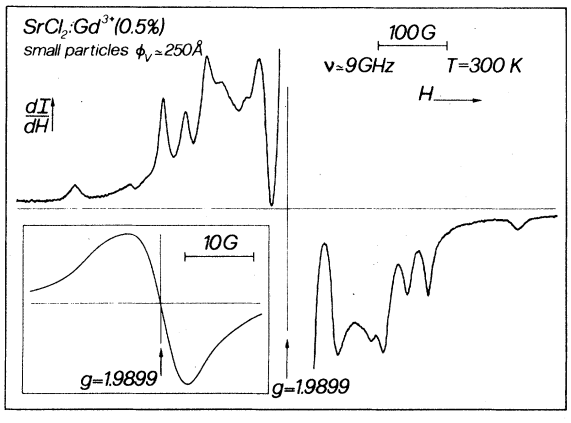

FIG. 13. EPR spectrum of the small-particle sample whose electron micrograph is shown in Fig. 6(b) (mean diameter $\phi_v = 250$ Å). The lines are now well resolved and the spin-Hamiltonian parameters obtained for this sample and reported in Table II approach those found for the bulk samples ($\Delta b_4/b_4 = 0.5\%$).

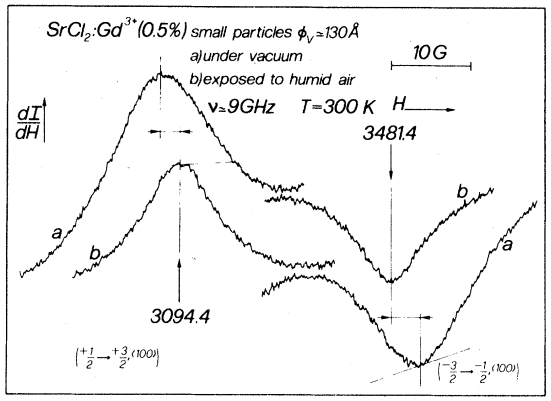

FIG. 14. Detail of the shoulders ($\pm\frac{3}{2} \leftrightarrow \pm\frac{1}{2}, \langle 100\rangle$) as measured for a small-particle sample with $\phi_v = 130$ Å: (a) when the sample has been protected from moist air in a sealed quartz tube (see the details of the collector in Fig. 5); and (b) when the sample was exposed to air for a few minutes.

$SrCl_2$ small particles is illustrated in the electron micrographs shown in Ref. 51.) This hydration-induced aggregation should not produce a repartition of the defects and a change in the defect density, while such changes could occur during the aggregation induced by a thermal treatment. Accordingly, if a size effect is operable, the shift Δb_4 should vanish (or almost vanish depending on the aggregate size) in the larger particles formed by the hydration-induced aggregation. The results of an experiment of this type are illustrated in Fig. 14, where the shoulders ($\pm\frac{3}{2} \rightarrow \pm\frac{1}{2}, \langle 100\rangle$) for a sample with $\phi_v = 130$ Å are compared with those observed after the sample had been exposed to air. The relative shift of $\Delta b_4/b_4 = 1.86\%$ found for the sample prior to the air exposure is reduced to only 0.23% after an exposure of a few minutes.[53] Based on the above cumulative evidence, it is possible to conclude that the observed increase in b_4 corresponds to a "size effect."

C. Positions and linewidths of the EPR shoulders as a function of particle size

The experimentally determined magnetic field separation $\Delta H^{sp}_{M,\langle 100\rangle}$ for $M = \frac{7}{2}, \frac{5}{2}$, and $\frac{3}{2}$ is shown in Fig. 15 as a function of the inverse of the small particle diameter ϕ_v. [The notation $\Delta H^{sp}_{M,\langle 100\rangle}$ employed here represents the magnetic field separation between conjugate pairs of transitions. With $M = \frac{7}{2}$, the separation would be measured between the ($-\frac{7}{2} \rightarrow -\frac{5}{2}, \langle 100\rangle$) and ($+\frac{5}{2} \rightarrow +\frac{7}{2}, \langle 100\rangle$) shoulders and so on.] It is clear from Fig. 15 that the position of the shoulders tends toward the bulk value (indexed as "B") as the particle size is increased.

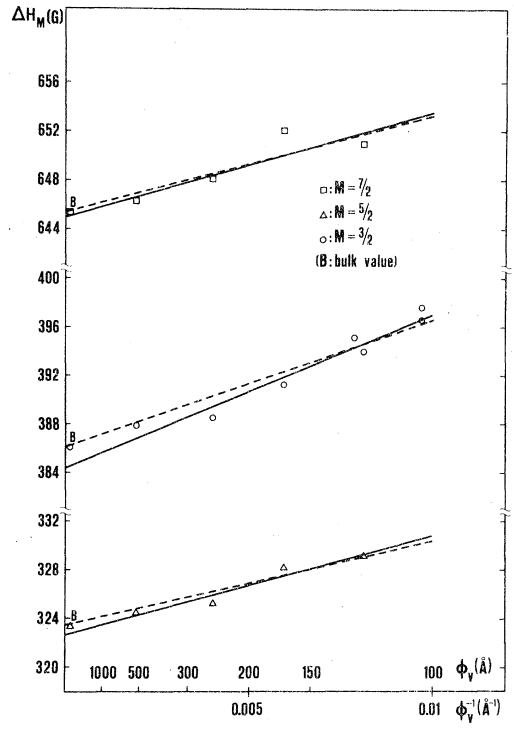

FIG. 15. Splitting ΔH_M of the shoulders ($\pm M \leftrightarrow \pm M \mp 1$, $\langle 100 \rangle$); with $M = \frac{3}{2}, \frac{5}{2}, \frac{7}{2}$, obtained for small-particle samples of $SrCl_2$:Gd^{3+} (0.5%) at X band and room temperature as a function of the inverse of the mean particle diameter ϕ_v. The dashed lines are least-squares fits which were obtained using the restriction that they approach the bulk values (indexed "B" at large particle sizes.) The straight lines correspond to least-squares fits for the small-particle samples only.

Electron-diffraction results obtained for small-particle samples are frequently interpreted by means of the so-called "drop model", which is only valid for an isotropic, spherical solid. In this model, the surface stress γ gives rise to a Laplace hydrostatic pressure and consequently to a lattice parameter contraction given by

$$\frac{\Delta a}{a} = \frac{1}{3}\frac{\Delta V}{V} = -\frac{2}{3}\frac{\beta\gamma}{R} = -\frac{4}{3}\frac{\beta\gamma}{\phi_v} \quad , \tag{15}$$

where β is the compressibility ($\beta = 3.10^{-11}$ m^2/N for $SrCl_2$) (Ref. 54). Assuming a power law of the form $b_4 \propto a^{-n}$, it is possible to deduce immediately that

$$\frac{\Delta b_4}{b_4} = -n\frac{\Delta a}{a} = \frac{4}{3}\frac{\beta\gamma n}{\phi_v} \quad . \tag{16}$$

Neglecting the b_6 parameter (which is almost zero, as can be seen from Table II), it is possible to write

$$\Delta H_{M,\langle 100\rangle} = C(M)\frac{b_4}{g\mu_B} \quad , \tag{17}$$

where $C(M)$ is equal to 40, 20, and 24, for $M = \frac{7}{2}$, $\frac{5}{2}$, and $\frac{3}{2}$, respectively [cf. Eq. (2) or Table I]. Therefore, based on this admittedly simple model, it is then possible to write

$$\Delta H^{sp}_{M,\langle 100\rangle} = \Delta H^{B}_{M,\langle 100\rangle} + \left(\frac{4}{3}\beta\gamma n\frac{b_4}{g\mu_B}\right)\frac{C(M)}{\phi_v} \quad . \tag{18}$$

The predicted linear dependence of $H^{sp}_{M,\langle 100\rangle}$ on ϕ_v^{-1} is approximately satisfied, as shown in Fig. 15. (The straight lines correspond to a least-squares fit to the small-particle values. The dashed lines have been obtained by imposing the requirement that the curves reach the bulk values.) The slope of the lines in Fig. 15 does not seem to vary with the $C(M)$ coefficients, however. In particular, the slope of the line for $M = \frac{7}{2}$ is too small in comparison with that obtained for $M = \frac{3}{2}$. It should be noted, however, that the shoulders ($\pm\frac{7}{2} \leftrightarrow \pm\frac{5}{2}$, $\langle 100\rangle$) are extremely difficult to measure accurately since their intensity is very weak (here the intensity minimum in the single-crystal spectrum also corresponds to the maximum spread of the intensity in the powder spectrum), and also the width of these shoulders is most sensitive to a distribution in the b_4 parameter. Using the results shown in Fig. 16, it can be shown that the relative change given by

$$\eta_M = \frac{\Delta H^{sp}_{M,\langle 100\rangle} - \Delta H^{B}_{M,\langle 100\rangle}}{\Delta H^{B}_{M,\langle 100\rangle}} = \frac{\Delta b_4}{b_4} \quad , \tag{19}$$

agrees quite well with the prediction of Eq. (18). A least-squares fit to the $\eta_M(\phi_v^{-1})$ values gives

$$\frac{\Delta b_4}{b_4} = \frac{3.2583}{\phi_v(\text{Å})} - 5.5\times 10^{-3} \quad .$$

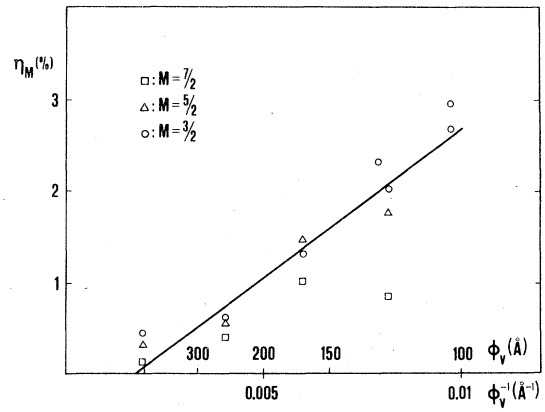

FIG. 16. Relative change $\eta_M = (\Delta H^{sp}_{M,\langle 100\rangle} - \Delta H^{B}_{M,\langle 100\rangle})/\Delta H^{B}_{M,\langle 100\rangle}$ of the $\Delta H_{M,\langle 100\rangle}$ splittings as a function of the inverse of the mean diameter ϕ_v of the small particles. By considering a pure hydrostatic compression and neglecting the b_6 parameter, the least-squares fit shown here gives the product $(n\gamma)$ directly. Here γ is the surface stress of $SrCl_2$ and n is the power-law exponent appropriate to the b_4 parameter.

The slope of this straight line corresponds to the following $(n\gamma)$ product:

$$(n\gamma) = 8.146 \text{ N/m} \ .$$

The negative intercept $\Delta b_4/b_4 = -5.5 \times 10^{-3}$ when $\phi_v \to \infty$ has no physical significance, since for $\phi_v = 500$ Å, the coefficient η_M is always positive and the slope of $\eta_M(\phi_v^{-1})$ appears to decrease. It is possible that this type of change could be correlated with a change in the small-particle habit, since in the sample with $\phi_v = 250$ Å [Fig. 6(b)], the largest crystals are faceted, while in the sample with $\phi_v = 500$ Å [see, for example, Fig. 2(a) of Ref. 51], all of the crystals have the shape of Wulff polyhedra.[55] Such a change in crystal habit (i.e., a non-Wulff-to-Wulff transition) would be in agreement with the remarks of Solliard and Buffat[9] concerning the difference between surface stress and surface tension when the surface planes are stretched.

The full width at half maximum $\Delta H_{1/2,M}$ of the shoulders $(\pm M \leftrightarrow \pm M \mp 1, \langle 100 \rangle)$ is shown in Fig. 17 as a function of ϕ_v^{-1}. Contrary to the spin-spin broadening effects illustrated in Fig. 19 (see Appendix D) the broadening of the shoulders for the small-particle samples is approximately proportional to their magnetic field separation from the "central" line $(-\frac{1}{2} \to +\frac{1}{2})$. In particular, the linewidths $\Delta H_{1/2,7/2}$ and $\Delta H_{1/2,5/2}$ are found to have the ratio 2:1, which corresponds reasonably well to the ratio $C(\frac{7}{2}):C(\frac{5}{2})$. These results indicate that the broadening is inhomogeneous and arises from a distribution in the b_4 parameter. A distribution in the fourth-order spin-Hamiltonian parameter could arise: (i) from a size distribution in the small $SrCl_2$ particles, (ii) from an inhomogeneous lattice contraction, or (iii) from the effects of multiple twinning.[18] These three possibilities will be treated in order as follows:

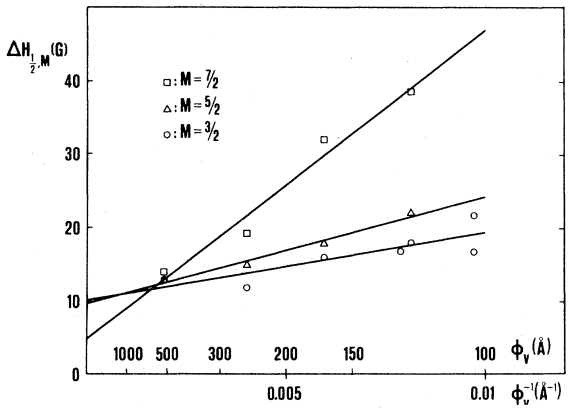

FIG. 17. Mean full width at half maximum $\Delta H_{1/2,M}$ of the two symmetric shoulders $(M \leftrightarrow M-1, \langle 100 \rangle)$ and $(-M \leftrightarrow -M+1, \langle 100 \rangle)$ as measured for small $SrCl_2$:Gd^{3+} particles. These values are reported as a function of the inverse of the mean diameter ϕ_v of the particles.

(i) If the position of a shoulder in the powder spectrum is given by Eq. (18), i.e., $H_M^{sp} = H_M^B + \alpha C(M)/\phi_v$, then a distribution $n(\phi)$ in the size of the crystals will result in an inhomogeneous broadening. If $\Delta\phi_{1/2}$ is the full width at half maximum (FWHM) of the size distribution $n(\phi)$, then the resulting broadening of the corresponding shoulder $\Delta H_{1/2,M}$ will vary as

$$\Delta H_{1/2,M} \approx \frac{\alpha C(M)}{\phi_v^2} \Delta\phi_{1/2} \ . \tag{20}$$

With the technique of evaporation in an inert gas employed in the present work, the size distribution is such that $\Delta\phi_{1/2} \approx \phi_v$. Consequently, the broadening due to a size distribution can be expressed as

$$(\Delta H_{1/2,M})_{n(\phi)} \approx \frac{\alpha C(M)}{\phi_v} \ . \tag{21}$$

For the shoulders $(\pm\frac{3}{2} \leftrightarrow \pm\frac{1}{2}, \langle 100 \rangle)$ in the spectrum of a sample with $\phi_v = 100$ Å, this represents a contribution of 5 G. The ϕ_v^{-1} dependence of $\Delta H_{1/2,M}$ predicted by Eq. (21) is in qualitative agreement with the values shown in Fig. 17. In order to deconvolute the line, however, a size histogram is required, and the determination of a reasonably representative histogram for particles such as those shown in Fig. 6(a) is not easy.

(ii) The lattice parameter may not necessarily be uniformly contracted inside a very small crystal. The surface atoms are certainly more perturbed relative to the atoms in the interior of the particle, and effects due to faceting of the particle should also be considered.[56] An additional complication could arise if the Gd^{3+} distribution were inhomogeneous (e.g., if a surface segregation of the impurities occurred).

(iii) Studies of the structure of small metallic particles (i.e., gold and silver) via the technique of electron microscopy have shown that, at thermodynamic equilibrium, the particles are characterized by a large number of twins.[17,18] No such evidence is present in our electron micrographs (e.g., Fig. 6). Using the statistical theory developed by Stoneham,[57] it can be shown[58] that the inhomogeneous broadening which would result from multiple twinning is of the same type as that produced by point defects. (That is, a Lorentzian line shape is predicted whose shift and width are linearly proportional to the twin density. In the case of multitwinned particles this density also varies as ϕ_v^{-1}.)

D. Correlation with the surface stress as measured by electron diffraction

In the present work, the technique of electron resonance has been established as a useful technique for the detection of the crystallographic size effect in small dielectric particles. Using the EPR technique alone, however, it is only possible (as noted in Sec.

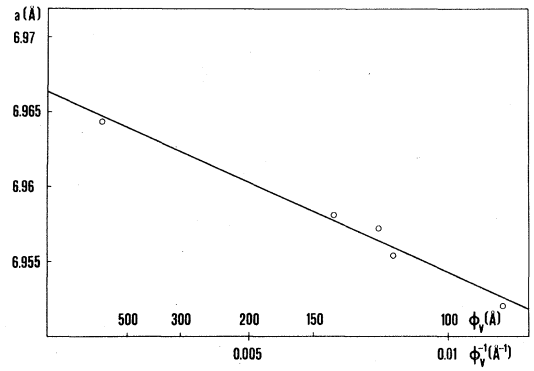

FIG. 18. Lattice parameter a of small $SrCl_2$:Gd^{3+} (0.1%) particles prepared by *in situ* evaporation on a heated substrate. The (422) Debye-Scherrer electron-diffraction ring was used for the determination of a. The a values are plotted here as a function of the inverse of the mean diameter ϕ_v of the small particles. The measurement technique is identical to that described previously in Ref. 9.

IV C) to deduce the product $(n\gamma)$. In order to separate the surface stress γ from the power-law exponent n, it is necessary to perform hydrostatic-pressure experiments on bulk samples, or to measure the lattice parameter contraction in small particles by diffraction techniques directly. The latter approach has been used in the present work, and the results obtained for samples formed by evaporation in vacuum (see Sec. III C) are shown in Fig. 18. The lattice parameter, which is shown as a function of the inverse of the particle diameter, was measured using the (422) Debye-Scherrer ring. The following result is obtained from a linear fit:

$$a(\text{Å}) = 6.9663 - \frac{1.2112}{\phi_v(\text{Å})} .$$

Using this result along with Eq. (15) we find that $\gamma = 0.435$ N/m. This value compares favorably with (a) the specific surface work as measured by cleavage at 77 K for BaF_2 [{111} plane, $\gamma = 0.28$ N/m at 298 K (Ref. 59)] and for CaF_2 [{111} plane, $\gamma = 0.45$ N/m at 298 K (Ref. 59)], and (b) the surface tension of molten[60] $SrCl_2$ ($\gamma = 0.17$ N/m at 1123 K and $d\gamma/dT \approx -7\times10^{-5}$ N/mK). It should be noted that the calculated surface tension[61] for the {111} planes in $SrCl_2$ is 2.63 N/m, which is significantly larger than the value of 0.435 N/m obtained here, while for the {110} planes, the calculated value is of the same order of magnitude (i.e., 0.319 N/m).

V. DISCUSSION AND CONCLUSION

From the combined EPR and electron-diffraction results obtained for small $SrCl_2$:Gd^{3+} particles, it is possible to deduce a power law of $b_4 \propto a^{-n}$, with $n = 18.7$ for the fourth-order crystal-field parameter. This exponent is apparently much larger than the exponent in the a^{-5} dependence predicted from a simple point-charge model.[62] The theoretical point-charge-model power law has been found to be quite different from the experimental determinations based on host-lattice variations, temperature variations, and hydrostatic-pressure experiments. The EPR results obtained for the fluorite-structure alkaline-earth fluorides (CdF_2, CaF_2, SrF_2, and BaF_2) result in a dependence on the host-lattice parameter of $a^{-3.5}$ and $a^{-2.02}$ for Eu^{2+} (Refs. 21 and 63) and Gd^{3+} (Refs. 20 and 64) ions, respectively. The use of these power laws to predict b_4 values for $SrCl_2$:Gd^{3+}, Eu^{2+} yields values which are much larger than the measured parameters,[29,65] however. Hurren *et al.*[21,66] have proposed that this discrepancy is due primarily to a local distortion of the host lattice around the paramagnetic impurity. For the $SrCl_2$:Gd^{3+} and SrF_2:Gd^{3+} systems, the local distortions should be nearly equivalent. [The distance $Sr^{2+}-Cl^-$ is 3.02 Å as compared to the sum of the ionic radii, $r(Gd^{3+})+r(Cl^-)=2.75$ Å, is "equivalent" to the Sr^{2+}–F^- distance of 2.51 Å compared to the sum of the ionic radii, $r(Gd^{3+})+r(F^-)=2.27$ Å.[67]] For these two systems an $a^{-5.4}$ dependence for the parameter b_4 is obtained, and this dependence agrees reasonably well with the hydrostatic-pressure measurements of Kasatochkin *et al.*,[20] who obtained values of $n = 7.2$, 6.5, and 7.4 for CaF_2, SrF_2, and BaF_2:Gd^{3+}, respectively. These values do not take into account any local distortion and are somewhat smaller than the values measured by Hurren *et al.*[21,66] for Eu^{2+} ions in the same hosts. It has been suggested that the exponent is smaller for Gd^{3+} due to a lattice contraction around the impurity ion, since, in this case, there is an excess positive charge. Temperature-variation measurements of the crystal-field parameter b_4, when interpreted in terms of a pure lattice dilatation, give rise to higher power laws. For the alkaline-earth fluorides, Rewaj[25] has found power laws of $b_4 \propto a^{-15}$ and a^{-20} for Gd^{3+} and Eu^{2+}, respectively.

The value of $n = 18.7$ obtained here for the $SrCl_2$:Gd^{3+} small-particle case could be explained in several different ways:

(i) Since the value is close to the exponents deduced from temperature-variation measurements, some dynamic phenomena could be involved. Effectively, the finite dimensions of the crystal produce a cutoff in the phonon spectrum. This cutoff can affect the spin-lattice relaxation time of the Gd^{3+} impurities, as our initial saturation measurements at 4.2 K appear to indicate. Dynamic effects can also change the value of the crystal-field parameters, since their temperature dependence reflects at least a 20 to 70%[23,24] dynamic contribution after substracting the amount due to the pure thermic dilatation.

(ii) For the smallest $SrCl_2$ crystals ($\phi_v \leq 250$ Å), the "real" structure is not known. They may be single crystals or may have internal twins similar to those

found in small metallic cubic-structure crystals. In any case, the smallest crystals must have nonuniform internal strains, since the surface planes are more distorted than the interior. The problem is the same for the largest crystals, which have a Wulff shape. Faceting effects[56] or nonuniform internal strains not only produce deviations from the very simple drop model, but also modify the form of the spin Hamiltonian of Eq. (1). If we consider, for example, a small b_2^0 axial term due to small distortions of the cubic sites, such terms could be important, as compared with changes in the b_4^0 parameter. This eventuality has not been considered here, since the EPR spectra corresponding to the small-particle samples (Figs. 9 and 13) were still apparently correlated to a cubic symmetry site.

(iii) Nonuniform strains as described in (ii) above can be combined with a surface segregation of the Gd^{3+} impurities. Some authors[68] have observed that Mn^{2+} impurities which were diluted in a single crystal of NaCl tended to diffuse toward the surface when the crystal was heated to 673 K. In our case, a surface segregation during the evaporation-thermalization process would give more weight to those sites close to the surface, and these are undoubtedly more distorted than the interior sites. Furthermore, the surface of the small $SrCl_2$ particles investigated here is certainly not "ultraclean", since ad- or absorbed layers of water are probably present with the conventional vacuum conditions (10^{-6} torr) used in these experiments.

In conclusion, the technique of electron paramagnetic resonance has been shown to be a useful technique for the detection and study of crystallographic size effects in small dielectric particles. This method is much more sensitive than electron-diffraction techniques; additionally, if the line shapes are deconvoluted with an accurate size histogram, it is possible to investigate effects due to defects and inhomogeneous strains.

ACKNOWLEDGMENTS

The authors are grateful to J.-P. Heger for his invaluable help with the computer programming, and to A. M. Stoneham and R. Lacroix for helpful discussions. The Interdepartmental Institute of Metallurgy of the Ecole Polytechnique Fédérale de Lausanne is also gratefully acknowledged for the use of the facilities for electron microscopy. This work was partially supported by the Swiss National Fund for Scientific Research under Grant No. 2.255-0.79. Oak Ridge National Laboratory is operated by Union Carbide Corporation with the U.S.DOE under Contract No. W-7405-eng-26.

APPENDIX A: METHOD OF LAGRANGIAN MULTIPLIERS

The extrema of the function [cf. Eq. (11)]

$$H(l,m,n)=\alpha[1-5(l^2m^2+m^2n^2+n^2l^2)]+\beta\{\tfrac{21}{2}[11l^2m^2n^2-(l^2m^2+m^2n^2+n^2l^2)+\tfrac{2}{21}]\} ,$$

may be calculated by introducing the function

$$\mathcal{L}(l,m,n,\lambda)=H(l,m,n)-\lambda(l^2+m^2+n^2-1)$$

and assuming that the extrema are given by

$$\frac{\delta\mathcal{L}}{\delta l}=\frac{\delta\mathcal{L}}{\delta m}=\frac{\delta\mathcal{L}}{\delta n}=\frac{\delta\mathcal{L}}{\delta\lambda}=0 .$$

(Note that the M subscript has been omitted for simplicity.) The results of this calculation are as follows:

$$-10\alpha l(m^2+n^2)+\tfrac{21}{2}\beta l[22m^2n^2-2(m^2+n^2)]-2\lambda l=0 . \quad \text{(A1)}$$

Plus circular permutations of (l,m,n) in Eq. (A1) above; and

$$l^2+m^2+n^2=1 . \quad \text{(A2)}$$

The conditions for the extrema are then determined to be either (a)

$$l=0 \quad \text{(A3)}$$

or (b)

$$\lambda=\tfrac{231}{2}\beta m^2n^2-(m^2+n^2)(5\alpha+\tfrac{21}{2}\beta) . \quad \text{(A4)}$$

Plus circular permutations of (l,m,n) in Eq. (A3) above; and

$$l^2+m^2+n^2=1 . \quad \text{(A5)}$$

These conditions are satisfied by the following three types of solutions:

(i) $l=m=0$ and $n=1$ { [001] direction }

($\lambda=0$ and $H=\alpha+\beta$)

(ii) $l=0$ and $m=n=\frac{1}{\sqrt{2}}$ { [011] direction }

($\lambda=-\frac{5}{2}\alpha-\frac{21}{4}\beta$ and $H=-\frac{1}{4}\alpha-\frac{13}{8}\beta$)

(iii) $l=m=n=\frac{1}{\sqrt{3}}$ { [111] direction }

($\lambda=-\frac{10}{3}\alpha+\frac{35}{6}\beta$ and $H=-\frac{2}{3}\alpha+\frac{16}{9}\beta$) .

These solutions correspond to the positions of shoulders and divergences determined from an exact calculation of $I_M^{p\delta}(H)$. The method of Lagrangian multipliers does not establish whether or not a given singularity corresponds to a shoulder or a divergence.

APPENDIX B: DETAILS OF THE POWDER-SPECTRUM CALCULATION

The position of a line (M) is given by the following expression [Eq. (11)]:

$$H = H_M(l,m,n) = \alpha_M[1-5(l^2m^2+m^2n^2+n^2l^2)] + \beta_M\{\tfrac{21}{2}[11\,l^2m^2n^2-(l^2m^2+m^2n^2+n^2l^2)+\tfrac{2}{21}]\} \ .$$

This expression must be used to calculate the integral $I_M^{P\delta}(H)$, which is given by

$$I_M^{P\delta}(H) = \int \frac{dn}{m\frac{\delta H}{\delta l} - l\frac{\delta H}{\delta m}} \ , \tag{B1}$$

where the conditions

$$l^2+m^2+n^2=1 \ ,$$

$$H = H_M(l,m,n) \ ,$$

are applicable. $H_M(l,m,n)$ may be transformed by using the following identity:

$$(l^2+m^2+n^2)^2 = 1 = (l^4+m^4+n^4) + 2(l^2m^2+m^2n^2+n^2l^2)$$

and the transformed expression is given by

$$H_M(l,m,n) = (\tfrac{5}{2}\alpha_M+\tfrac{21}{4}\beta_M)(l^4+m^4+n^4) + \tfrac{231}{2}\beta_M l^2m^2n^2 - (\tfrac{3}{2}\alpha_M+\tfrac{17}{4}\beta_M) \ .$$

This equation may be written as

$$H' = H'_M(l,m,n) = A_M(l^4+m^4+n^4) + B_M l^2m^2n^2 \ ,$$

where

$$H' = H + \tfrac{3}{2}\alpha_M + \tfrac{17}{4}\beta_M \ ,$$

$$A_M = \tfrac{5}{2}\alpha_M + \tfrac{21}{4}\beta_M, \quad B_M = \tfrac{231}{2}\beta_M \ .$$

When this expression is substituted in Eq. (B1) above, the following integral is obtained:

$$I_M^{P\delta}(H') = \int \frac{dn}{l\,m(l^2-m^2)(4A_M - 2B_M n^2)} \ ,$$

with

$$l^2+m^2+n^2=1 \ ,$$

$$H' = A_M(l^4+m^4+n^4) + B_M(l^2m^2n^2) \ .$$

We must now express l and m, or more precisely, lm and (l^2-m^2) as a function of H' and n. By writing

$$F = l^4+m^4 = \frac{H' - A_M n^4 - B_M \frac{1}{2}n^2(1-n^2)^2}{A_M - \frac{1}{2}B_M(n^2)} \ ,$$

it is easy to show that

$$lm = \left[\frac{(1-n^2)^2 - F}{2}\right]^{1/2}$$

and

$$(l^2-m^2) = [2F-(1-n^2)^2]^{1/2} \ .$$

When these expressions are substituted into $I_M^{P\delta}(H')$ and the following definitions are made:

$$\epsilon_M = \frac{B_M}{2A_M} = \frac{231\beta_M}{10\alpha_M+21\beta_M}$$

and

$$h_M = \frac{H'}{A_M} = \frac{H+\frac{3}{2}\alpha_M+\frac{17}{4}\beta_M}{\frac{5}{2}\alpha_M+\frac{21}{4}\beta_M} \ ,$$

the following expression for the integral of Eq. (B1) is obtained:

$$I_M^{P\delta}(h_M) \sim (\tfrac{5}{2}\alpha_M+\tfrac{21}{4}\beta_M)^{-1}\int \frac{dn}{f_M(n,h_M)} \ ,$$

with

$$f_M(n,h_M) = (2n^4-2n^2+1-h_M)^{1/2} \times [2h_M - (3n^4-2n^2+1) - \epsilon_M n^2(n^4-2n^2+1)]^{1/2} \ .$$

APPENDIX C: DOMAIN OF DEFINITION OF THE FUNCTION $f_M(n,h_M)$

The domain of definition of the function

$$f(n,h) = [g_2(n,h)]^{1/2}[g_3(n,h)]^{1/2} \ ,$$

with

$$g_2(n,h) = 2n^4-2n^2+1-h$$

and

$$g_3(n,h) = 2h-(3n^4-2n^2+1)-\epsilon n^2(n^4-2n^2+1) \ ,$$

is given by the zeros of g_2 and g_3, and this domain is shown in Fig. 1 for $\epsilon=0$. (Here the index M has been suppressed.) The effect of a nonzero value of ϵ on the domain must now be determined. First, it should be noted that the domain limit corresponding to the biquadratic expression g_2 is independent of ϵ; and, second, that the term which multiplies ϵ in the expression g_3 can be rewritten as

$$n^2(n^4-2n^2+1) = [n(n-1)(n+1)]^2 \ .$$

This term is zero for $n=0, \pm 1$; and the shoulder $h=1$, $(H=\alpha+\beta)$ and the divergence $h=1/2$, $(H=-\alpha/4-\frac{13}{8}\beta)$ always arise from the $\langle 100\rangle$ and $\langle 110\rangle$ directions, respectively. The second shoulder $(h=\frac{1}{3}$ if $\epsilon=0)$ corresponding to the minimum of h on the line $g_3(n,h)=0$ is given by the following two conditions:

$$(1)\ g_3(n,h)=0\ ,$$

$$(2)\ \frac{dh}{dn}=0 \quad \text{with } g_3(n,h)=0\ .$$

The second condition is equivalent to

$$\frac{\partial g_3(n,h)}{\partial n}=0=-6\epsilon n^5+4n^3(2\epsilon-3)+2n(2-\epsilon)\ .$$

The solutions of this equation are: $n=0$, which is a relative maximum $h=\frac{1}{2}$; $n^2=(1-2/\epsilon)$, which is to be rejected since it diverges when $\epsilon\to 0$; and $n^2=\frac{1}{3}$. By using the solution $n^2=\frac{1}{3}$ along with the condition $g_3(n,h)=0$ we immediately obtain the result: $h=(9+2\epsilon)/27$ and, therefore, $(H=-2\alpha/3+16\beta/9)$. This shoulder corresponds to $\langle 111\rangle$ directions.

APPENDIX D: SPIN-SPIN BROADENING

The position of a shoulder in the powder pattern is deduced, as noted in Sec. III C, by fitting a Lorentzian line shape superimposed on a linear base to the experimental spectrum. It is necessary to establish that the position of the shoulder (i.e., the center of the Lorentzian) is independent of the linewidth in order to prove that the increased separation between the $(-\frac{3}{2}\to-\frac{1}{2}, \langle 100\rangle)$ and $(+\frac{1}{2}\to+\frac{3}{2}, \langle 100\rangle)$ transitions does not arise simply due to the effect of overlapping shoulders. For this purpose, the linewidths and positions of shoulders in large-grain $SrCl_2$:Gd^{3+} powders have been measured in samples where the Gd^{3+} concentration was varied from 0.05% to 2%. Grant and Strandberg[69] have shown that, for concentrations in this range, the resulting spin-spin broadening is Lorentzian and is linearly dependent on the concentration of the paramagnetic impurities. A dependence of this type is shown at the top of Fig. 19 for the shoulders $(\pm\frac{3}{2}\leftrightarrow\pm\frac{1}{2}, \langle 100\rangle)$ and $(\pm\frac{7}{2}\leftrightarrow\pm\frac{5}{2}, \langle 100\rangle)$. It should be noted that this broadening does not depend on whether the transitions are $(\pm\frac{3}{2}\to\pm\frac{1}{2}, \langle 100\rangle)$ or $(\pm\frac{7}{2}\to\pm\frac{5}{2}, \langle 100\rangle)$ while, as the results show, the line broadening observed for small-particle samples is such that the linewidth of a shoulder is proportional to its magnetic field position. For large-grain powders, the magnetic field separations ΔH_M between the shoulders $(-\frac{3}{2}\to-\frac{1}{2}, \langle 100\rangle)$ and $(+\frac{1}{2}\to+\frac{3}{2}, \langle 100\rangle)$ and between the $(-\frac{7}{2}\to-\frac{5}{2}, \langle 100\rangle)$ and $(+\frac{5}{2}\to+\frac{7}{2}, \langle 100\rangle)$ shoulders are shown in the bottom portion of Fig. 19, and these separations do not depend on the concentration of Gd^{3+}.[70] Therefore, the experimentally observed increase in the magnetic field separation between the $(-\frac{3}{2}\to-\frac{1}{2}, \langle 100\rangle)$ and $(+\frac{1}{2}\to+\frac{3}{2}, \langle 100\rangle)$ shoulders for the small-particle samples does not arise from line-broadening effects.

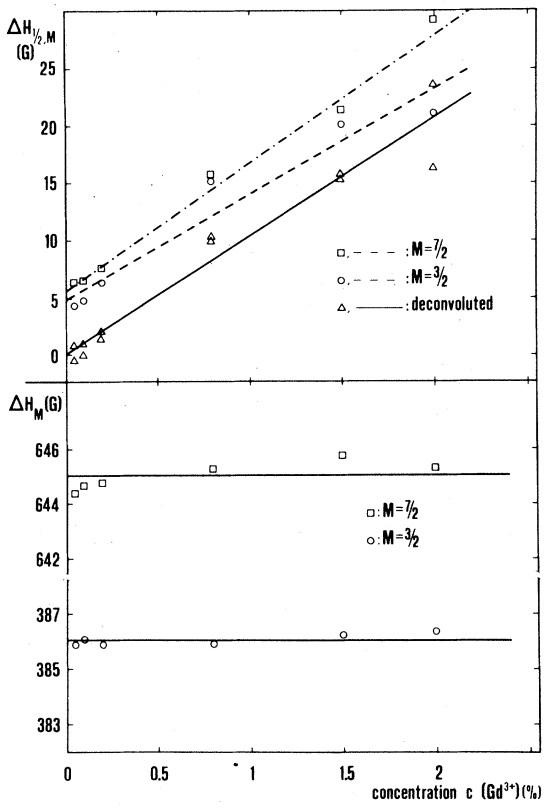

FIG. 19. $\Delta H_{1/2,M}$ values, which are shown as a function of the Gd^{3+} concentration, correspond to the mean full width at half maximum of the two symmetric shoulders $(M\leftrightarrow M-1, \langle 100\rangle)$ and $(-M\leftrightarrow -M+1, \langle 100\rangle)$ where $M=\frac{3}{2},\frac{7}{2}$. These values were obtained by the same fitting technique used in the case of the small-particle samples. The spin-spin broadening observed for large-grain powders appears to be linearly dependent on the Gd^{3+} concentration and is not significantly different for different electronic transitions. This situation contrasts with the broadening observed for small-particle samples (see Fig. 17). At the bottom of the figure, it can be seen that the splitting ΔH_M of these shoulders is independent of the Gd^{3+} concentration.

*Present Address: Solid State Division, Oak Ridge National Laboratory, Oak Ridge, Tennessee 37830.

[1]R. Kubo, J. Phys. Soc. Jpn. 17, 975 (1962). See also: R. Kubo and A. Kawabata, J. Phys. Soc. Jpn. 21, 1765 (1966); A. Kawabata, J. Phys. Soc. Jpn. 29, 902 (1970).

[2]J. P. Borel and J. L. Millet, J. Phys. (Paris) 38, C2-115 (1977), and references therein.

[3]S. Kobayashi, J. Phys. (Paris) 38, C2-121 (1977), and references therein.

[4]M. A. Smithard, Solid State Commun. 14, 407 (1974), and references therein.

[5]F. Piuz and J. P. Borel, Phys. Status Solidi A 14, 129 (1972), and references therein.

[6]Th. F. Nonnenmacher, Phys. Lett. A 51, 213 (1975), and references therein.

[7]Th. F. Nonnenmacher and R. Wunderle, Phys. Status Solidi B 82, 257 (1977), and references therein.

[8]Ph. Buffat and J. P. Borel, Phys. Rev. A 13, 2287 (1976), and references therein.

[9]C. Solliard and Ph. Buffat, J. Phys. (Paris) 38, C2-167 (1977).

[10]F. W. C. Boswell, Proc. Phys. Soc. London Sect. A 64, 465 (1951).

[11]C. W. Mays, J. S. Vermaak, and D. Kuhlmann-Wilsdorf, Surf. Sci. 12, 134 (1968). See also: Surf. Sci. 22, 164 (1970); 32, 168 (1972).

[12]T. de Planta, R. Ghez and F. Piuz, Helv. Phys. Acta 37, 74 (1964).

[13]M. M. Nicolson, Proc. R. Soc. London Sect. A 241, 376 (1957).

[14]M. M. Nicolson, Proc. R. Soc. London Sect. A 228, 490 (1955).

[15]A. Cimino, P. Porta, and M. Valigi, J. Am. Ceram. Soc. 49, 152 (1965).

[16]R. C. Garvie, Mater. Res. Bull. 1, 161 (1966).

[17]C. Solliard, Ph. Buffat, and F. Faes, J. Crystal Growth 32, 123 (1976).

[18]S. Ino, J. Phys. Soc. Jpn. 21, 346 (1966). See also: J. Phys. Soc. Jpn. 22, 1365 (1967); J. Phys. Soc. Jpn. 27, 941 (1969); J. Vacuum Sci. Technol. 6, 527 (1969).

[19]A preliminary note has been published in: J. Phys. (Paris) 38, C2-105 (1977).

[20]S. V. Kasatochkin, T. I. Alaeva, E. N. Yakovlev, and L. F. Vereshchagin, Sov. Phys. Solid State 15, 229 (1973).

[21]W. R. Hurren, H. M. Nelson, E. G. Larson, and J. H. Gardner, Phys. Rev. 185, 624 (1969).

[22]W. Urban, Phys. Status Solidi B 46, 579 (1971).

[23]S. B. Oseroff and R. Calvo, J. Phys. Chem. Solids 33, 2275 (1972).

[24]R. Calvo, R. A. Isaacson, and Z. Sroubek, Phys. Rev. 177, 484 (1969).

[25]T. Rewaj, Sov. Phys. Solid State 9, 2340 (1968); 10, 1014 (1968).

[26]M. M. Abraham and L. A. Boatner, J. Chem. Phys. 51, 3134 (1969).

[27]R. Lacroix, Helv. Phys. Acta 30, 374 (1957).

[28]The method of Lagrangian multipliers is very similar to the standard technique described for example in: I. V. Ovchinnikov and V. N. Konstantinov, J. Magn. Reson. 32, 179 (1978).

[29]M. M. Abraham, L. A. Boatner, and E. J. Lee, Phys. Lett. A 25, 230 (1967).

[30]*American Institute of Physics Handbook,* 3rd ed. (McGraw-Hill, New York, 1972), p. 4-244.

[31]I. Barin and O. Knacke, *Thermochemical Properties of Inorganic Substances* (Springer, Berlin, 1973), p. 708.

[32]*Handbook of Chemistry and Physics,* 51st ed. (Chemical Rubber, Cleveland, 1970-71), p. B142.

[33]P. Pascal, *Nouveau Traite de Chimie Minerale* (Masson, Paris, 1958), Vol. IV, p. 633.

[34]*Gmelins Handbuch, Der Anorganischen Chemie* (Verlag Chemie, Berlin, 1960), Vol. 29, p. 196.

[35]*Crystals with the Fluorite Structure,* edited by W. Hayes (Oxford University Press, New York, 1974), p. 114.

[36]Landolt - Börnstein, *Crystal Structure Data of Inorganic Compounds* (Springer, Berlin, 1973), Group III, Vol. 7, Part a, p. 374.

[37]R. W. G. Wyckoff, *Crystal Structures* (Interscience, New York, 1963), Vol. 1, p. 239.

[38]M. Shand, R. C. Hanson, C. E. Derrington, and M. O'Keeffe, Solid State Commun. 18, 769 (1976).

[39]S. Lee, C. C. Yang, and A. J. Bevolo, Phys. Rev. B 10, 4515 (1974).

[40]C. C. Yang, S. Lee, and A. J. Bevolo, Phys. Rev. B 12, 4687 (1975).

[41]R. W. Reynolds, Ph.D. thesis (Vanderbilt University, 1969) (unpublished).

[42]H. A. Buckmaster and Y. H. Shing, Phys. Status Solidi A 12, 325 (1972).

[43]*Handbook of Chemistry and Physics,* 51st ed. (Chemical Rubber, Cleveland, 1970-71), p. B390.

[44]K. Kimoto, Y. Kamiya, M. Nonoyama, and R. Uyeda, Jpn. J. Appl. Phys. 2, 702 (1963).

[45]T. Hayashi, T. Ohno, S. Yatsuya, and R. Uyeda, Jpn. J. Appl. Phys. 16, 705 (1977). A detailed list of the work carried out in Japan since 1963 using the technique of evaporation in a gaseous atmosphere is given in the references in this article.

[46]D. Boscarato, Diplôme du Laboratoire de Physique Expérimentale, Ecole Polytechnique Fédérale de Lausanne, Switzerland (1974) (unpublished).

[47]D. M. Mann and H. P. Broida, J. Appl. Phys. 44, 4950 (1973). See also: J. Appl. Phys. 45, 596 (1974).

[48]J. D. Eversole, K. Sakurai, and H. P. Broida, J. Cryst. Growth 33, 353 (1976).

[49]M. Rappaz and F. Faes, J. Appl. Phys. 46, 3273 (1975).

[50]J. D. F. Ramsay and R. G. Avery, J. Mater. Sci. 9, 1681 and 1689 (1974).

[51]C. Solliard and M. Rappaz, Rev. Sci. Instrum. 49, 101 (1978).

[52]From the broadening of the diffraction peaks shown in Fig. 12, a particle size of 65 Å can be determined if a Gaussian line shape is assumed, and 115 Å if a Lorentzian line shape is used. These values correspond quite well to the particle size of 100 Å deduced from the electron micrographs.

[53]It should be noted that an exposure of a $SrCl_2$:Gd^{3+} powder sample to the air for several hours can be used to observe complete hydration of the crystals by EPR techniques. [See: M. Rappaz, J. Chem. Phys. (to be published).] The EPR spectrum, which initially corresponds to the cubic symmetry of anhydrous $SrCl_2$ (as shown in Fig. 8), is transformed, following the completion of the hydration process, into a spectrum which is typical of the trigonal symmetry site of $SrCl_2 \cdot 6H_2O$:Gd^{3+}.

[54]H. V. Lauer, Jr., K. A. Solberg, D. H. Kühner, and W. E. Bron, Phys. Lett. A 35, 219 (1971).

[55]R. Defay, I. Prigogine, A. Bellemans, and D. H. Everett,

Surface Tension and Adsorption (Longmans, Green, New York, 1966), p. 296.
[56]A. M. Stoneham, J. Phys. C 10, 1175 (1977).
[57]A. M. Stoneham, Rev. Mod. Phys. 41, 82 (1969).
[58]M. Rappaz, Ph.D. thesis (Ecole Polytechnique Fédérale de Lausanne, 1978) (unpublished).
[59]Ed. M. Green, *Solid State Surfaces Science* (Dekker, New York, 1973), Vol. 2, p. 86.
[60]G. Bertozzi and G. Soldani, J. Phys. Chem. 6, 1838 (1966).
[61]A. M. Stoneham (private communication).
[62]See, for example: A. Abragam and B. Bleaney, *Electron Paramagnetic Resonance of Transition Ions* (Oxford University, New York, 1970), Chap. 16.
[63]H. J. Gläser and D. Geist, Z. Naturforch. 20a, 842 (1965).
[64]J. M. Baker and F. I. B. Williams, Proc. R. Soc. London Sect. A 267, 283 (1962).
[65]R. W. Reynolds, L. A. Boatner, and M. M. Abraham, J. Chem. Phys. 52, 3851 (1970).
[66]W. R. Hurren, Ph.D. thesis (Brigham Young University, 1968) (unpublished).
[67]Z. I. Ivanenko and B. Z. Malkin, Sov. Phys. Solid State 11, 1498 (1970); 11, 981 (1969).
[68]M. J. Yacaman and A. G. Rodriguez, Philos. Mag. 32, 13 (1975).
[69]W. J. C. Grant and M. W. P. Strandberg, Phys. Rev. 135, A715 and A727 (1964).
[70]At high gadolinium concentrations some Gd^{3+} ions will have Gd^{3+} neighbors 4.93 Å away along a $\langle 110 \rangle$ direction. The EPR spectrum for these Gd^{3+}–Gd^{3+} complexes would then have C_{2v} symmetry but, such a spectrum would be too weak to be observed in a powder sample.

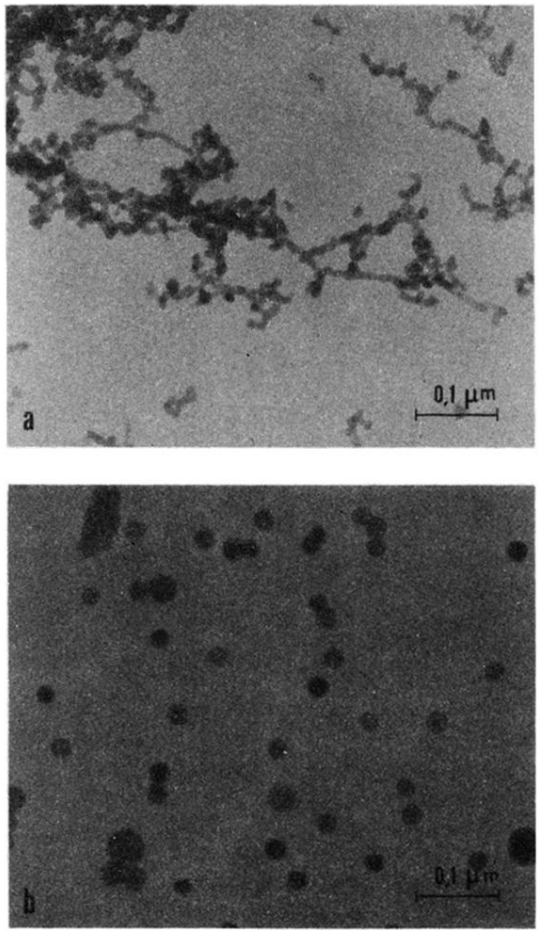

FIG. 6. Electron micrographs of the small $SrCl_2:Gd^{3+}$ particles produced with the apparatus illustrated in Fig. 5. The argon pressure (10 torr) and flow rate (5.62 torr l/sec) are the same for the two samples. In this way, the average size ϕ_v of the particles can be controlled by the evaporation temperature alone. (a) $T_e = 1373$ K and $\phi_v = 100$ Å; (b) $T_e = 1658$ K and $\phi_v = 250$ Å. It should be noted that the smallest particles, as shown in *a*, are arranged in chainlike structures, while the larger particles illustrated in *b* are well isolated.